“Characterizing aerosol transport into the Canadian High Arctic using aerosol mass spectrometry and Lagrangian modelling” by T. Kuhn et al.

Our responses to comments are shown in italics.

ACPD, 10, C4075–C4076, 2010
Anonymous Referee #1

Nice and ambitious paper which presents interesting results from the high Canadian Arctic. The measurements from the PEARL will be of great and increased interest to the science community when the time period of the data has grown large enough to perform reliable statistical analysis. Its high altitude location may give crucial information in the years to come if the data is combined with the ones from e.g. Alert, another Canadian Arctic station, when it comes to characterizing to what extent the stratification of the Arctic troposphere affects what source regions that are sampled in the measurements at different heights.

Some small comments: Throughout the paper be consistent in the use of “l/min” or “l min-1”. Choose one and stick with it.
We have fixed that in revised manuscript, we thank the reviewer for noticing.
Also replaced “l” with “L” to avoid confusion between “1” (number) and “l” (letter) regardless of font used; left “ml” unchanged.

Page 13408 Line 8: “long range” missing a “-”
We have fixed that in revised manuscript.

P.13409 L.22: “sources of these materials” “.” is missing.
We have fixed that in revised manuscript..

P.13413 L.7: Definition of the expression “ID”.
“inner diameter (ID)”; we have fixed that in revised manuscript.

P.13415 L.12-13: “Of course, the particles are very well: : :” Consider revising.
The revised statement will be “The particles are heated to the same temperature as the air, because heating of particles by collisions with air molecules is fast compared to transport times through the inlet.” or something equivalent in updated manuscript.

P.13418 L.25-26: “These data are shown in green on Fig. 4.” Should be “in Fig. 4.”
We have fixed that in revised manuscript.

P.13419 L.11-17: “Data from the first: : : : : a correlation coefficient R2=0.50” Consider reformulate this part to make it more clear for the reader, and consider the use of the word “points” in this section.
The first group, which has $SO_4^=$ concentrations above 0.5 $\mu g\ m^{-3}$ (episode between 1 September 2006 01:00 UTC and 3 September 2006 13:00 UTC) shows a different trend than points with SO_4 below about

0.4 μg m^{-3}. The second group, between 2 October 2006 and 12 October 2006 (shown in green on the scatter plot in Fig.~5 and having SO_4 concentrations below 0.4 μg m^{-3}) have a higher correlation coefficient, R^2=0.50, than during other periods.

P.13420 L.25: Definition of the expression "MS mode".
The definition of MS and TOF modes are given in the AMS literature (eg. Jimenez et al. 2003). Instead of reiterating these, we will ad references on P. 13416, L. 10-13: "The averaged aerosol mass spectrum, acquired in the MS mode (Jimenez et al., 2003), and size distributions of selected species, acquired in the TOF mode (Jimenez et al., 2003) are saved each hour …."

P.13423 L.21: "(called the source: : :" missing the end of this parenthesis.
We have fixed that in revised manuscript.

P.13424 L.12,17 & P.13441 Figure caption Fig.9: Which dates are plotted and discussed, 20-23 or 26-29 of August?
The dates for the clean air are 20-23 August, hence the Figure caption Fig.9 will be changed to "20 August 2006-00:00z to 23 August 2006-21:00z".

P.13424 L.26 (Fig. 10): ": : : areas distributed over Russia." From the plots it is really hard to see if these footprint residence times are only located over Russia as described. It looks like a major part of this "Russian" contribution might be more properly assigned also to the Baltic States, Belarus, Ukraine and Kazakhstan. This will then also have an effect on the section where conclusions are drawn.
This and similar comments from referee #2 suggested to us that our original analysis of the Lagrangian calculations was not sufficiently thorough. Consequently, we looked again at these results more carefully under higher resolution. This analysis resulted in a more precise identification of the source regions, which led to the separation of the high sulfate episodes shown in Figure 2 into three separate parts. Appropriate modifications were made to the text describing Figure 2. Section 4.1, which describes the Lagrangian calculations, was completely rewritten and the related parts of the Conclusions section were also rewritten. Figures 10 and 11 were revised and Figure 12 was added. We believe this has added to the value of the manuscript and we thank the referee for stimulating this additional work.

P.13425 L.20-21: ": : : as well from central and western Russia". See comment made above about the interpretation of Fig. 10.
See response above related to Fig. 10.

P.13425 L. 23: "throughput" Misspelling?
Correct spelling in Oxford Dictionary is "throughput".

P. 13426 L.18: See comment above about the interpretation of Fig. 10.
See response above related to Fig. 10.

ACPD, 10, C5089, 2010
Anonymous Referee #2

I believe the manuscript is well written and summarizes first set of results from measurements made in Canadian high Arctic, at a site that is mostly in the free troposphere.
However, I see one fundamental problem with the measurements of semi-volatile aerosol species (i.e., organic aerosols and ammonium nitrate) after heating the samples up to 20 degrees C. With ambient temperature at the site being only slightly above freezing, if at all, in Aug-Oct, heating of the sample by at least 15-20 degrees C can very well drive off most of the aerosol phase ammonium nitrate and most likely organics to the gas phase. Therefore, I'm not sure the measurements truly reflect the amount of organics and ammonium nitrate transported to the site as they are described currently in the paper. Since the authors have done a very good analysis on particle transmission through the inlet, I suggest they expand the modeling exercise to estimate how much of the semivolatiles could have been evaporated in the sampling line with this temperature increase.
Then, they should very clearly explain this artifact in the manuscript and reflect the effect of this artifact in the conclusions drawn from measurements of nitrate and organics (Currently the authors discuss this only briefly on P13418). Measurements of sulfate on the other hand should be robust and artifact-free.
The reviewer identifies a very important consideration for all measurements that sample in low temperature environments. By way of clarification, we have extended our discussion of this issue in Section 2.2 as follows:

The mean residence time of air in our inlet system is approximately 25 s (determined from the flow speed in the sampling tubes). This relatively low residence time is achieved by choosing a high flow rate in the 7.2 m straight sampling pipe. It assures that sampling losses due to evaporation of the more volatile aerosol components remain small. For example, direct measurements (Bergin et al. 1997, ES&T 31 (10), pp2878) show that there would be less than 10% loss of pure ammonium nitrate aerosol in 25 s at 20 degrees C. This is an upper limit for the loss in our measurement, since evaporation will be even slower for internally mixed aerosol (Stelson and Seinfeld 2007, AE 41 (Suppl. 1) pp.126).

Also, we have modified Section 3.1 as follows:
"…we note that if inorganic nitrate ***in the form of ammonium nitrate*** *were present, it is possible that it might be partially re-partitioned from the aerosol to the gas phase during transit through the room temperature inlet following sampling from cold ambient conditions. If this occurred, the inorganic component would be underestimated* ***(by less than 10%, see Sect. 2.2)****. In view of the discussion at the beginning of this section, however, it is clear that ammonium nitrate aerosol is negligible during the sampling period.* ***Inorganic nitrate may be present in other forms than ammonium nitrate. Teinilä et al. 2004 found that during their measurements on Svalbard nitrate salts were most likely*** $NaNO_3$ ***and*** $Ca(NO_3)_2$***, which are non-volatile. They also show additional evidence that nitrate evaporation losses have been minimal during their campaign."***

Our nitrate concentrations were on average only 6% of our sulfate concentrations.This is consistent with previous measurements of Arctic aerosol. Covert and Heintzenberg 1993 observed

a ratio of nitrate to sulfate mass concentrations in aerosol with aerodynamic diameter less than 2.5 µm of less than 0.05; Parungo et al. 1993 (AE 27 (17-18), pp2825) detected sulfate in almost all particles they collected during flights in the planetary boundary layer over the Arctic, whereas only less than 1% of the particles contained nitrate; Teinilä et al. 2003 observed a nitrate to sulfate ratio of approximately 0.05 during their "light" campaign (measurements after polar sunrise). In addition, Teinilä et al. 2003 observed that most nitrate was found in supermicrometer particles (~90%), whereas most sulfate was found in submicrometer particles (~90%). Teinilä et al. 2004 confirmed this also at Zeppelin site on Svalbard.

From the above discussion we expect low nitrate concentrations, confirming our AMS measurements in the submicrometer range, and we do not suspect significant losses of inorganic nitrate.

We have also modified: "There is, however, a good correlation between nitrates and organics that persists through the whole dataset. This suggests strongly that the ***majority of the*** *small nitrate mass concentrations that were observed stem from organic nitrates.* ***This will be discussed further in the next section (3.2).****"*

I also think the manuscript lacks support in 2 other areas:
First, I would like to see some comparison of these measurements with other Arctic aerosol measurements in the US or Canada (for similar times of the year) just to put the current measurements in perspective.
For comparison we have added results from other Arctic aerosol measurements, such as :

"Sirois and Barrie 1999 (JGR 104, D9, pp11599) report 15 years weekly average measurements of aerosol composition at Alert, 150 km north-east of PEARL. Sulfate was the dominant aerosol component with average concentrations of around 1 µg m^{-3} in winter and maximum of 2 µg m^{-3} in spring time. In summer it drops to a minimum of just below 0.1 µg m^{-3} in July and August, then starts to increase again and reaches about 0.2 µg m^{-3} in October. Hence, our average sulfate concentrations are very similar compared to the August-October values of this nearby station. Both nitrate and ammonium concentrations at Alert were roughly one tenth or less of the sulfate measurements and featured a similar seasonal trend but somewhat less pronounced than the sulfate one. Both species have minimum average concentrations in September at around 0.02 µg m^{-3}. This is similar to our average ammonium and somewhat higher than our nitrate measurements. Other major components at Alert were the refractory species Na, Cl, Al, Ca, and Mg (with concentrations similar to ammonium and nitrate), which cannot be measured with the AMS.
Sirois and Barrie 1999 could distinguish two sulfate components, neutralized ammonium sulfate and acidic sulfate, of which the latter was dominant after polar sunrise, presumably due to increased photo-oxidation of SO_2. This is also consistent with our findings of acidic sulfate, with the episodes of very acidic sulfate corresponding to periods of increased SO_2 transport to our site (as we show with FLEXPART analysis).
Measurements from Greenland are reported by Heidam et al. 1993 (AE, 27(17-18), pp3029). The semi-weekly average concentrations from four years have similar seasonal trends as observed at Alert. Sulfate was also in Greenland the predominant component with average concentrations

between 0.1 and 0.3 μg m^{-3} during the August-October period, quite similar to our measurements."
Comparison with other Arctic measurements, not necessarily including the summer period, have been added to the discussion of our results where appropriate, e.g. discussion of potential volatility losses, aerosol acidity, or organic/inorganic nitrate.

Second, I would like to see more discussion on meteorological differences of the two highlighted time periods which resulted in transport of pollution to the site- but with very different footprints according to FLEXPART.
As explained in the response to Referee 1, we have completely rewritten Section 4.1, which describes the FLEXPART results. This and similar comments from Referee 1 suggested to us that our original analysis of the Lagrangian calculations was not sufficiently thorough. Consequently, we made a more precise identification of the source regions, which led to the separation of the high sulfate episodes shown in Figure 2 into three separate parts. Appropriate modifications were made to the text describing Figure 2. Also, Figures 10 and 11 were revised and Figure 12 was added, so that now these figures give the results for the new subdivision into episodes 1, 2a and 2b, respectively. We believe this has added to the value of the manuscript and we thank the referees for stimulating this additional work.
Regarding the differences in meteorology: the Lagrangian simulations were run for 20 days and the detailed meteorology varied considerably during that time, so it is difficult to identify the specific meteorological patterns that were most important in causing the differences in the footprints. Of course, FLEXPART integrates over the entire simulation time and thus includes all of the meteorological variations that occur during that time. We have, however, noted the large scale features of the meteorology in the rewritten Section 4.1

Overall, I think the measurements are important because the site has the potential to become a long-term measurement site in the high Arctic in free troposphere and help understand the transport of pollutants to the arctic.
I recommend publishing the manuscript after the revisions suggested above and below are addressed.
1. P13408. line 18, "…with 'an' average …."
Opening bracket at wrong place, should read: "… with on average 0.11 μg m^{-3} (detection limit…)".

2. Abstract- specifically when reporting average values of organics and nitrate explain the sampling artifact discussed above and note that these average values are lower limits by ***%.
We have added the following sentence after line 15 of the Abstract: "The air temperature was raised to about 20 C during sampling, but the short residence time in the inlet system (~25s) ensured that less than 10% of semivolatiles such as ammonium nitrate were lost."

3. P13412, line 25- note that 80 and 700 nm are in vacuum aerodynamic space.
Will add "… 700 nm vacuum aerodynamic diameter (Liu et al., 2007)".

4. What is the chopper duty cycle? Indicate this in the manuscript. Since a window within the poly-dispersed distribution of particles is chosen for IE calibrations,

what do you think the uncertainty in size of particles in that window is and how does that affect the estimated IE? Do you imply that the fact that the poly method gives 10-15% lower IE values is because of this uncertainty in size of particles?
The chopper duty cycle is 1% (and it operates at about 150 Hz).
Both methods, our "TOF window-within-polydisperse" method and the ususal "mobility-diameter-monodisperse" method (using a differential mobility analyzer, DMA) will have an uncertainty in size of particles. The different methods used to select particles of a certain size (together with perhaps different uncertainties) are most likely responsible for the systematic differences observed in estimated IE during calibration. By selecting a TOF window, using a filter function (by modyfing the AMS software algorithm) that resembles the shape of the monodisperse calibration aerosol sampled by the DMA, our method could perhaps yield results closer to the monodisperse method. Since we currently have no access to a DMA, we suggest that other AMS users perform such intercomparisons. The results could be valuable in situations where a DMA is not available (or may be down for repairs).

5. P13418- about nitrate signal- the authors hint here and also on P13420 that the nitrate signal is not really inorganic nitrate. I suggest using the observed ratio of 46/30 from mass calibrations to estimate amount of inorganic nitrate (left) on the aerosols and then assigning the rest of the signal to organics (either organic nitrate or other organics with interferences at m/z=30). This procedure was previously explained in Bae et al. (Interference of organic signals in highly time resolved nitrate measurements by low mass resolution aerosol mass spectrometry, JGR, Vol. 112, D22305, doi:10.1029/2007JD008614, 2007).
We already discussed this ratio briefly in the manuscript concluding that most of nitrate is organic nitrate. We will add to this discussion:
*"Relatively low ratios of NO_2^+ :NO^+ **(the two major nitrate fragments at m/z=46 and m/z=30; this ratio was 0.37** on average) are a further indication that organic nitrate aerosol accounts for most of the measured nitrate (Fry et al., 2009). During calibration of the AMS with ammonium nitrate this ratio is around 1. These organic nitrates are most likely formed during transport and are responsible for the observed good correlation between nitrate and organics. This would also explain the different sulfate-nitrate trend that we pointed out above for data with sulfate concentrations higher than 0.5 µg m . These data were measured during an exceptionally high sulfate episode around 2 September 2006 that was accompanied by a modest increase in the concentration of organics (see Fig. 2).*
Bae et al. 2007 (doi:10.1029/2007JD008614) suggested determining inorganic nitrate from m/z=46 only by using the 46/30 ratio from calibration and assigning the remaining fraction of m/z=30 to organics. When applying this to our data, the inorganic nitrate as well as the organic part of the AMS nitrate measurement are both still correlated to organics (R^2=0.6). Therefore, our discussions about nitrate are still valid even if we consider this inorganic nitrate only. The average concentration of inorganic nitrate is 0.03 µg m^{-3} (compared to the total nitrate 0.07 µg m^{-3}).

6. P13419, Because it's likely that most of the 'nitrate' signal is from organics, I don't see an advantage of discussing correlation of sulfate and 'nitrate'. I suggest revisiting the correlations after calculating the 'excess nitrate' as suggested in (5). Furthermore, again because of the heating of the sample line, I'm not sure if good

or bad correlation of organics or sulfate with inorganic nitrate will be any conclusive if no correction for evaporation of semivolatile species is considered.
After removing organic nitrate as suggested in (5.), correlations of inorganic nitrate with other species (including sulfate) are still similar. In addition, as explained above, we don't expect large losses of inorganic nitrate, and hence our discussion is still valid.

7. P13420, what collection efficiency was used to estimate mass of species by AMS? Since there are definitely episodes of highly acidic sulfate (or sulfuric acid) particles, the nominal CE=0.5 can not be applied.
As in other studies where most aerosol was expected to be internally mixed (Alfarra et al. 2004, Rupakheti et al. 2004) we did not apply species-dependent collection efficiencies.
In case of the episodes of sulfate/sulfuric acid particles this may lead to overestimating the concentrations. This would not affect our discussion and conclusions drawn, however, since the episodes are so pronounced with an up to tenfold increase in concentration.

8. P13421, line 5, was the pToF nitrate mode based on m/z=30 or 46? If m/z=30 has a lot of interference from organics, then this 'nitrate' mode is again not inorganic nitrate.
Both m/z30 and 46 were used. If only 46 is used then data are too noisy to clearly see the mode.
We have modified the manuscript to reflect these considerations.
Nitrate has been removed from Fig. 8, where nitrate concentrations were not sufficient to show a size distribution.

9. P13425, Ohio river valley is also a big contributor to SO_2 in eastern US. It is hard to see specifically in Fig 10 if the Ohio region has also influenced the trajectories, but it is worth zooming onto the map and verifying that (in this case, add it to line 19).
As discussed above, we have re-examined the FLEXPART results and rewritten the entire Section 4.1, in which the FLEXPART source identification is discussed, as well as the related parts of the Conclusions.

10. P13425, I am confused about the oil refinery numbers presented here. If Siberia puts out ~9.8 Mbbl of oil/day, how can the total Russian output be about half of that?! Are these two numbers mis-typed?
This information was not included in the rewritten Section 4.1, but for the information of the referee, the difference in these numbers reflects the fact that most of the oil produced in Russia is refined abroad.

11. P13425, Consider adding "…so losses to the atmosphere are larger than 'what would' occur with more …" to line 24-25.
Has been added.

12. Are there any gas phase measurements (like CO2, CO, NOy, O3, etc…) that can be added to the current analysis when looking at back trajectories? That will greatly strengthen the conclusions drawn from FLEXPART in terms of anthropogenic influence on the transported pollution.

Unfortunately, such gas phase measurements are not available.

13. Fig 2-3: I recommend adding measurements of ambient temperature, RH (or dew Pt) and sampling inlet temperature to the time series.
Ambient temperature and RH measured at PEARL were not included because they did not show any significant correlations with the data. We have attached time series plots of temperature/RH to this response. Inlet temperature was monitored and controlled to 20degC, however, we do not have logged data for the period we are reporting in this paper.

14. I would remove Fig 5 and 6.
Given our discussion and conclusion about the validity of the nitrate or inorganic nitrate correlations with other species we think it is important to keep these figures.

15. Fig 9-11: It's very hard to see anything in the bottom panels. Consider having these in larger sizes.

In the revised manuscript, the lower panels of Figures 10 – 12 have been plotted at larger scales.

The attached figures supplement pt. 13. above.

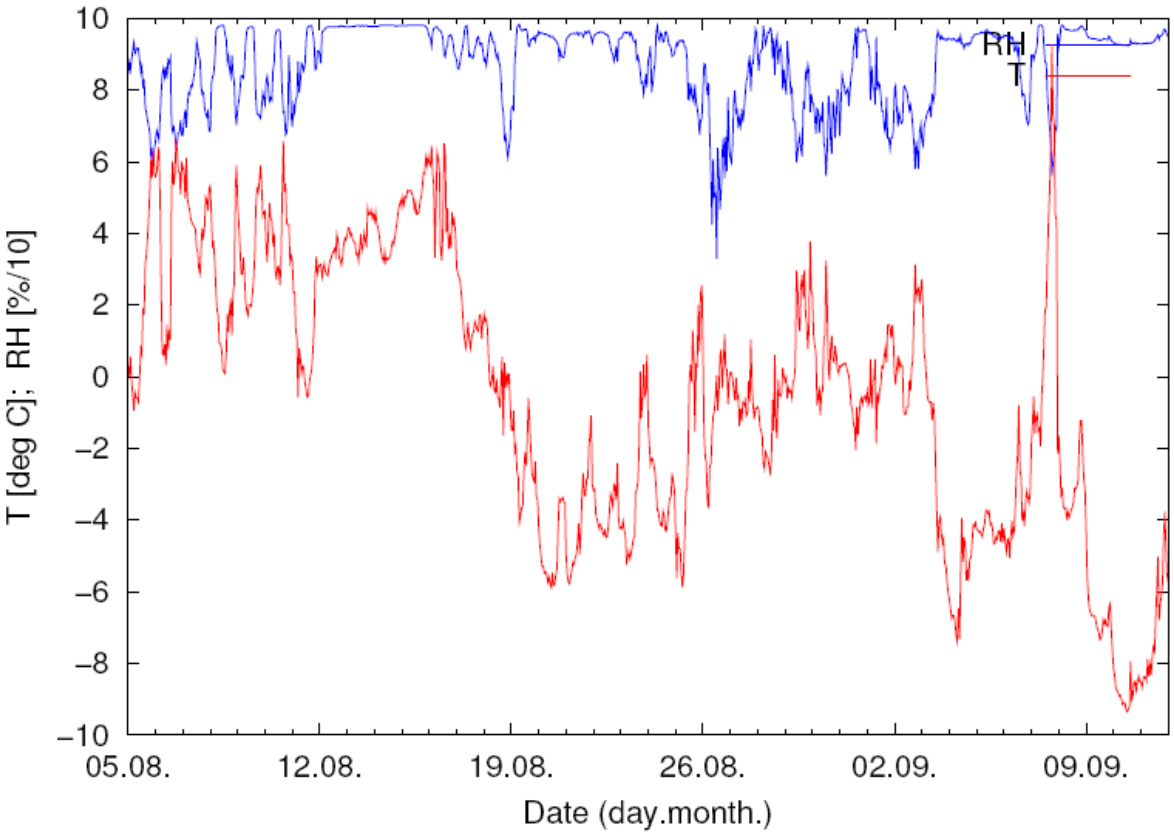

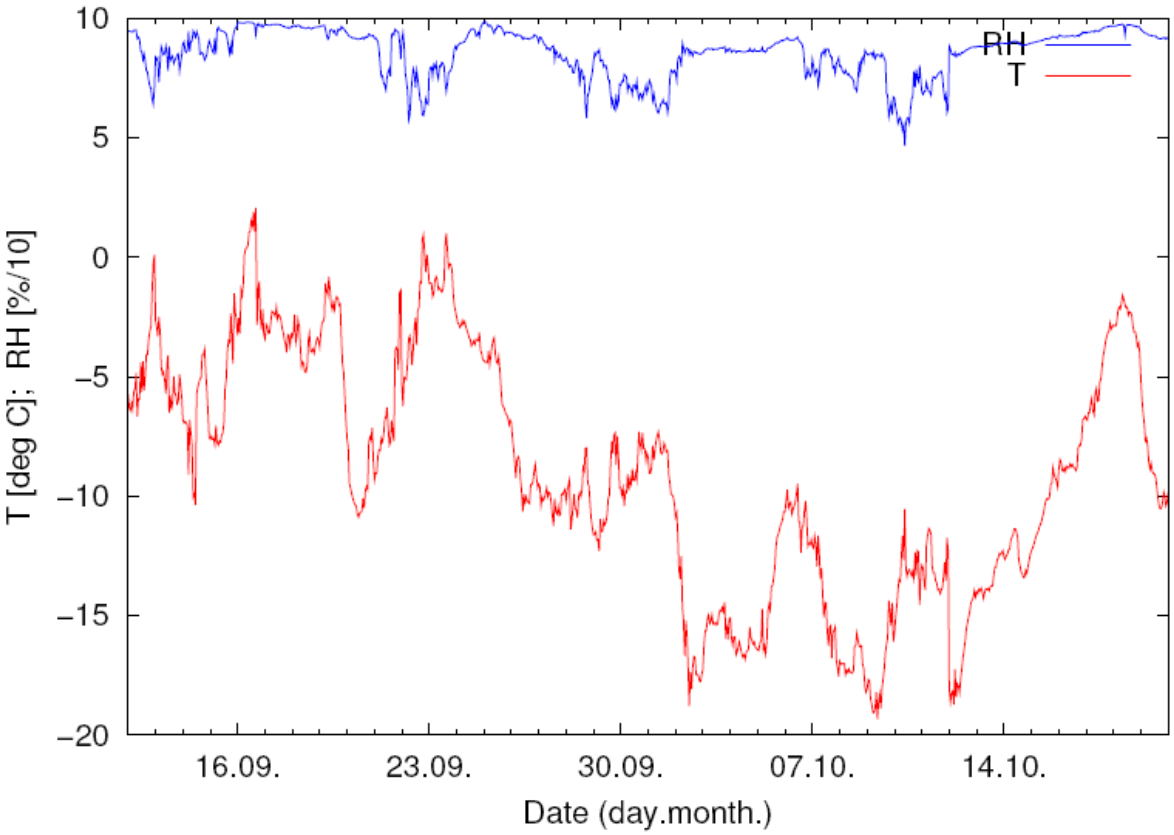
10
5
0
−5
−10
−15
−20
T [deg C]; RH [%/10]
16.09.
23.09.
30.09.
07.10.
14.10.
Date (day.month.)
RH
T

Characterizing aerosol transport into the Canadian High Arctic using aerosol mass spectrometry and Lagrangian modelling

T. Kuhn[2)]; R. Damoah[1)]; A. Bacak[3)] and J. J. Sloan[1)]

[1)]Department of Earth and Environmental Sciences
University of Waterloo,
Waterloo, ON N2L 3G1, Canada

[2)]Department of Space Science, Luleå University of Technology, Kiruna, Sweden

[3)]School of Earth, Atmospheric and Environmental Sciences, The University of Manchester,
Williamson Building, Oxford Road,
Manchester, M13 9PL, UK.

Corresponding author
J. J. Sloan
Tel.: +1 519 888 4401; fax: +1 519 746 7484.
E-mail address: sloanj@uwaterloo.ca (J.J. Sloan).

Abstract

We report the analysis of measurements made using an aerosol mass spectrometer (AMS; Aerodyne Research Inc.) that was installed in the Polar Environment Atmospheric Research Laboratory (PEARL) in summer 2006. PEARL is located in the Canadian high Arctic at 610 m above sea level on Ellesmere Island (80°N 86°W). PEARL is unique for its remote location in the Arctic and because most of the time it is situated within the free troposphere. It is therefore well suited as a receptor site to study the long-range tropospheric transport of pollutants into the Arctic. Some information about the successful year-round operation of an AMS at a high Arctic site such as PEARL will be reported here, together with design considerations for reliable sampling under harsh low-temperature conditions. Computational fluid dynamics calculations were made to ensure that sample integrity was maintained while sampling air at temperatures that average -40°C in the winter and can be as low as -55°C. Selected AMS measurements of aerosol mass concentration, size, and chemical composition recorded during the months of

August, September and October 2006 will be reported. The air temperature was raised to about 20°C during sampling, but the short residence time in the inlet system (~25 s) ensured that less than 10% of semivolatiles such as ammonium nitrate were lost. During this period, sulfate was at most times the predominant aerosol component with on average 0.115 μg m^{-3} (detection limit 0.003 μg m^{-3}). The second most abundant component was undifferentiated organic aerosol, with on average 0.11 μg m^{-3} (detection limit 0.04 μg m^{-3}). The nitrate component, which averaged 0.007 μg m^{-3}, was above its detection limit (0.002 μg m^{-3}), whereas the ammonium ion had an apparent average concentration of 0.02 μg m^{-3}, which was approximately equal to its detection limit. A few episodes having increased mass concentrations and lasting from several hours to several days are apparent in the data. These were investigated further using a statistical analysis to determine their common characteristics. High correlations among some of the components arriving during the short term episodes provide evidence for common sources. Lagrangian methods were also used to identify the source regions for some of the episodes. In all cases, these coincided with the arrival of air that had contacted the surface at latitudes below about 60^{o} N. Most of these lower-latitude footprints were on land, but sulfate emissions from shipping in the Atlantic were also detected. The Lagrangian results demonstrate that there is direct transport of polluted air into the high Arctic (up to 80^{o}N) from latitudes down to 40^{o}N on a time scale of 2-3 weeks. The polluted air originates in a wide variety of industrial, resource extraction and petroleum-related activity as well as from large population centres.

Keywords: Arctic; atmospheric aerosol; submicron particles; mass size distribution; chemical composition, Lagrangian modelling

1 Introduction

The Arctic is a relatively pristine environment, but it is not completely isolated from distant anthropogenic influences. Information about transport of pollution into the Arctic is documented regularly in the reports of the Arctic Monitoring and Assessment Programme (AMAP), which identify the large-scale tropospheric pathways whereby pollutants are brought from low to high latitudes (AMAP, 2003). One of the most dramatic consequences of this pollution, Arctic haze, is associated with the intrusion of polluted air into the Arctic in winter and spring, when anthropogenic sources and the Arctic are within the same (cold) air masses (Heintzenberg, 1989). Related to this, early measurements showed that anthropogenic aerosols from low latitudes are an important component of Arctic contamination (Hoff et al., 1983). Possibly more important are semi-volatile organic pollutants like pesticides which, like the aerosols, have no high latitude sources, yet are found in high concentrations at many Arctic locations (e.g. Bailey et al., 2000;Halsall et al., 1998;Hung et al., 2005;Oehme, 1991;Oehme and Ottar, 1984). The presence of these clearly identifiable contaminants demonstrates the existence of transport pathways for anthropogenic pollutants into the Arctic.

Much work has been done during more than two decades to identify the sources of these materials. This effort is made more difficult by recent indications that the predominant locations of emission sources may be changing (Hung et al., 2005;Sirois and Barrie, 1999). Some reports suggest that these originate in regions of Eurasia, but parts of North America have also been indicated for some receptor locations (Halsall et al., 1997;Nyeki et al., 2005;Pacyna, 1995;Polissar et al., 2001;Xie et al., 1999). For these reasons and many others relating to the health of the affected communities, it is important to continue the efforts to monitor and understand long range transport of pollutants into the Arctic.

Particulate matter (PM) in the smaller size ranges (*e.g.* PM_1), which is transported over long distances (Saarikoski et al., 2008;Sehili and Lammel, 2007), is a useful tracer for the origins of this material as well as a vector for transport of contaminants (Lammel et al., 2009). Many of the important effects occur at Arctic sunrise when photochemical processes begin after months of darkness. Aerosols also cause important radiative effects in the Arctic. For example, increases in the number and size of sulfate aerosols from photo-oxidation of SO_2 can cause

surface cooling by reflecting incoming radiation (Hung et al., 2005;Sirois and Barrie, 1999), whereas aerosols of other sizes and compositions can have warming effects. Thus there is a strong connection between the chemical compositions of aerosols and their radiative effects.

There have been many studies of the chemical compositions of Arctic aerosols (e.g. Covert and Heintzenberg, 1993;Heidam et al., 1993;Heintzenberg and Leck, 1994;Sirois and Barrie, 1999;Staebler et al., 1999), some of which also report particle size information (Barrie et al., 1994;Hillamo et al., 2001;Ricard et al., 2002;Teinilä et al., 2003). Not all studies include organic matter, which is a significant fraction of the aerosol (Heintzenberg, 1989) and studies that do include organics usually focus only on toxics like pesticides (Hung et al., 2005) or selected compounds such as dicarboxylic acids (e.g. Narukawa et al., 2002;Teinilä et al., 2003), thereby omitting most of the organic mass fraction.

Finally, most Arctic measurement sites represented in the data referenced above are at or close to sea level, which is a disadvantage when studying long range transport occurring in the free troposphere. Exceptions to this include the Zeppelin site close to Ny-Ålesund on Svalbard, which at 474 m a.s.l., is located in the free troposphere for much of the time. This site has been used for measurements of aerosol chemical composition in several studies (Heintzenberg and Leck, 1994;Ström et al., 2003;Teinilä et al., 2004). Clearly, it is desirable to have more measurements of aerosol size and composition in the high Arctic. Additionally, the temporal variation of these parameters is less well characterized than the average values and this is also an extremely important factor to explore.

In the following, we report selected measurements of the temporal variations in aerosol size and composition that were carried out at the Polar Environment Atmospheric Research Laboratory (PEARL) in the Canadian Arctic. Located at 80°02’N, 86°15’W at an elevation of 610 m, PEARL is in the free troposphere and thus is ideally suited for studying aerosol transport into the Arctic. The measurements were done using an aerosol mass spectrometer (AMS; Aerodyne Research Inc.) that provides a continuous data record with high temporal resolution. These measurements are the first recorded by an AMS in the Arctic and, to the knowledge of the authors, they represent the first time that ground-based real-time chemical analysis of Arctic aerosols has been attempted. We describe here the sampling site and some design features of the

installation that were necessitated by the need to ensure the integrity of the samples under the harsh conditions of the PEARL laboratory. Computational fluid dynamics (CFD) simulations of the inlet system are reported, to verify that particles in the size range that can be detected by the instrument were sampled efficiently. We also report analyses by several methods of episodes relevant for studies of long range transport. Statistical analyses and Lagrangian modelling of these were used to provide information about common sources and geographical locations.

2 Site and Installation Details

2.1 Polar Environment Atmospheric Laboratory (PEARL)

The PEARL laboratory is a facility of the Canadian Network for the Detection of Atmospheric Change (CANDAC) in the Canadian high Arctic. It is located on Ellesmere Island in Nunavut, Canada, 9 km west from Eureka (79°59'N, 85°56'W), which is a Canadian High Arctic Weather Station (HAWS). About two kilometres east of the weather station is the Eureka airport and a small military base. Eureka is 160 km north of the nearest community (Grise Fjord) and about 150 km south-west of the Canadian Forces Station (CFS) Alert, which is home to a more substantial military presence, as well as another HAWS. The PEARL laboratory is located on top of a 610 m ridge, a few kilometres east of Eureka Sound, which runs North-South, and just north of Slidre Fjord, which runs East-West. The neighbouring hills are at similar or lower altitudes, so the laboratory is located within the free troposphere almost all of the time. These geographical features make PEARL an ideal and unique site for an Arctic observatory.

Between 1993 and 2002, the facility, then called the Arctic Stratospheric Observatory (AStrO), was used by Environment Canada (EC) for (mostly) stratospheric observations. The Arctic atmospheric research program at PEARL was initiated under new funding from the Canada Foundation for Climate and Atmospheric Studies (CFCAS), the Canada Foundation for Innovation (CFI), the Ontario Innovation Trust (OIT), and the Atlantic Innovation Fund (AIF)/Nova Scotia Research Innovation Trust (NSRIT). Several new CANDAC programs made possible by this funding have expanded the research scope into the lower atmosphere. Since

summer 2005, PEARL has been operated year-round by CANDAC. One to three operators maintain the facility and oversee the experiments. Electric power for the laboratory is produced in Eureka by a diesel generating plant, which is located away from the prevailing wind direction, so measurements at PEARL are not affected by local pollution sources, another important asset of the laboratory.

2.2 AMS Installation

An AMS from Aerodyne Research Inc. (Canagaratna et al., 2007;Jayne et al., 2000;Jimenez et al., 2003) was installed at PEARL in August 2006. The AMS provides near real-time size resolved composition analysis of non-refractory particulate matter in the size range from approximately 80 nm to 700 nm vacuum aerodynamic diameter (Liu et al., 2007). During operation, particles are aerodynamically focused in a high-vacuum system (Liu et al., 2007) onto a heated surface (temperature ~ 540°C) where non-refractory components are thermally vaporised and analysed by electron impact (70 eV) ionization quadrupole mass spectrometry. The instrument at PEARL (a 215 series AMS) has a particle time of flight (TOF) path of 293 mm and a critical orifice diameter of 0.1 mm, which fixes the inlet flow rate at approximately 1.3 cm^3 s^{-1} (≈80 ml min^{-1}).

The AMS is operated at a normal room temperature of approximately 20°C inside the PEARL laboratory. An air stream of 11 L min^{-1} (laboratory temperature and pressure) is sampled through an inlet assembly located about 2.2 m above the roof of the laboratory and flows to the AMS through a 22 mm inner diameter (ID) stainless steel inlet pipe, which is approximately 7.2 m long. The flow rate and pipe dimension results in laminar flow with a Reynolds number (Re) of approximately 700. Close to the AMS, the flow is split in three parts: a 1 L min^{-1} flow to the AMS and two 5 L min^{-1} flows, which can be used to sample total suspended particles (TSP) and PM_1 on filters. (The latter measurements will not be reported here.) The 1 L min^{-1} flow is transferred to the inlet of the AMS through a 37 cm long, 5.2 mm ID stainless steel tube at Re ≈ 300. A stainless steel tube approximately 15.5 cm long and 2 mm ID sub-samples the AMS inlet flow rate of 80 ml min^{-1} from the core of the 1 L min^{-1} flow and delivers it to the critical orifice of the AMS inlet. This sub-sampling is slightly sub-isokinetic; the mean speed in the 2 mm ID sampling tube is approximately half of the mean speed in the 5.2 mm ID tube with the 1 L min^{-1}

flow. This however, does not present a problem, because the inertia of 1 μm particles is negligible (Stokes' number Stk = 0.001 for 1 μm particle with density of water and 2 mm ID sampling tube). Thus the sub-sample of 1 μm and smaller particles is representative of the sample in the 1 L min^{-1} flow.

Figure 1 shows a 30° radial section through the inlet assembly on the laboratory roof. The outer surface is an inverted, heated cylindrical cup (120 mm ID), which is insulated on the outside. The cup surrounds the inlet pipe, which is flared slightly at the top to resemble a funnel, with a 38.1 mm diameter top opening that narrows to 25.4 mm at the bottom. Both the funnel and the cover are maintained at a temperature of 20 °C in order to bring the sampled air to room temperature quickly when it enters the inlet. This removes larger ice crystals that might otherwise not evaporate completely before being sampled by the AMS (Staebler et al., 1999). After passing through the inlet assembly, air enters the inlet pipe, which passes through a 10 cm diameter, 3 m long PVC tube mounted in an insulated hatch in the roof of the room where the AMS is located.

Care was taken to ensure that the sampling system would work properly, even for the lowest (-55 ^{o}C) outside temperatures encountered in the winter. The temperature changes caused by bringing the sampled air to the temperature of the AMS inlet could cause buoyancy effects, which might give rise to convective recirculation of the sampled air stream inside the inlet pipe. For simple flow geometries it is sufficient to estimate the effects of buoyancy using the buoyancy parameter, Gr/Re^2 (Incropera and DeWitt, 1999), which is a dimensionless number that compares the strength of buoyant forces with that of inertial forces using a characteristic length (the tube diameter) and temperature difference (here the difference between wall and gas temperatures). When Gr/Re^2 is smaller than unity, the flow is dominated by inertial forces and buoyancy can be neglected. In case of the main inlet pipe, in which the flow is 11 L min^{-1}, even a temperature difference of 60 °C between the tube wall and the gas would only result in a buoyancy parameter of 0.2. For typical temperature differences of about 10 °C, the buoyancy parameter would be 0.03, so buoyancy inside the main inlet pipe is not important and we can safely neglect it.

198 The inlet assembly leading to the funnel at the top of the inlet pipe is designed to raise the
199 temperature of the sample from that of the (possibly very cold) ambient outside air to that of the
200 AMS. Since the flow speeds are slowest in this region, the inertial forces are weakest and it is
201 not possible to exclude convective recirculation simply on the basis of the buoyancy parameter,
202 which in this case is larger than unity. Therefore, we have modeled the flow in the inlet
203 assembly using computational fluid dynamics (CFD) (ANSYS CFX; ANSYS 11.0, ANSYS Inc.
204 Canonsburg, PA, USA).

205 Figure 1 shows the CFD-calculated trajectories of 1 μm diameter particles (density of 1000 kg m^{-3})
206 that were released across the cross section of the opening at the bottom of the inlet. For this
207 purpose, the air entering the opening was assumed to have a temperature of -40 °C. The CFD
208 analysis shows that buoyant forces cause the air and particles to rise faster in the proximity of the
209 heated walls than in the other parts of the inlet. This draws the particles closer to the heated
210 wall, enhancing the heat transfer to them and directing them to the region above the inlet pipe,
211 from which they are swept into the top of the funnel. The air in the central region of the gap
212 between the inlet pipe and the heated can is nearly stagnant. The slow circulation there does not
213 affect particles in the size range detectable by the AMS (approximately 80 nm to 700 nm).
214 Particles larger than about 25 μm (aerodynamic diameter) are eliminated in the inlet by
215 elutriation (they are too heavy and are not carried up into the inlet), while particles with
216 diameters of 10 μm or smaller have transmission efficiency through the inlet region of 100%.

217 The CFD results also verified the effective heating of air in the inlet. The air inside the funnel
218 reaches a temperature ≥ 15°C when the sampled air is at -40°C if the inlet wall is kept at 20°C.
219 The particles are heated to the same temperature as the air, because heating of particles by
220 collisions with air molecules is fast compared to transport times through the inlet.

221 After entering the inlet pipe, the air flows through three 90° bends before being sampled by the
222 AMS: the first is a Swagelok Tee where 6 L min^{-1} is taken from the 11 L min^{-1} inlet flow; the
223 second is a 90° elbow; and the third is another Tee, where 1 L min^{-1} is split from the 6 L min^{-1}
224 flow. At a flow rate of 6 L min^{-1}, losses at a 90° bend in a tube with ID of 22 mm
225 (approximating the first Swagelok Tee) are very close to zero. For particles of 10 μm
226 aerodynamic diameter, the transport efficiency through the bend is 99% (Hinds, 1999). This may

also be confirmed directly from the fact that the Stokes numbers in this flow for particles having diameters less than 10 μm are much smaller than unity (approximately $6 \cdot 10^{-3}$ and $7 \cdot 10^{-5}$ for 10 μm and 1 μm particles respectively). Hence particles smaller than 1 μm, which is above the upper limit for detection by the AMS, will follow the air stream without problems. Similar calculations confirm that losses in the other two bends for particles smaller than 10 μm are also close to zero, a result that was also confirmed using CFD modelling of particle flow through these bends.

Diffusion losses in the sampling line were also evaluated using (Gormley and Kennedy, 1949). The 11 L min^{-1} flow through the 7.2 m long sampling pipe yields a transmission efficiency of 99.3% for 70 nm particles (below lower detection limit of AMS, which detects particles of about 80 nm with a 50% efficiency (Liu et al., 2007)). Transmission efficiencies in the sections having 6 L min^{-1} and 1 L min^{-1} flows are even higher. The 15.5 cm long tube through which the AMS samples with its 80 ml min^{-1} flow has the lowest transmission efficiency with 98.6% for 80 nm particles. Overall, the diffusion losses should amount to about 3% for particles with 70 nm diameter and losses for larger particles are smaller.

The mean residence time of air in our inlet system is approximately 25 s (determined from the flow speed in the sampling tubes). This relatively low residence time is achieved by choosing a high flow rate in the 7.2 m straight sampling pipe. It assures that sampling losses due to evaporation of the more volatile aerosol components remain small. For example, direct measurements (Bergin et al., 1997) show that there would be less than 10% loss of pure ammonium nitrate aerosol in 25 s at 20°C. This is an upper limit for the loss in our measurement, since evaporation will be even slower for internally mixed aerosol (Stelson and Seinfeld, 2007).

2.3 Sampling protocol

For the results reported here, the AMS operated continuously using a one-hour signal averaging cycle. The averaged aerosol mass spectrum, acquired in the MS mode (Jimenez et al., 2003), and size distributions of selected species, acquired in the TOF mode (Jimenez et al., 2003) are saved each hour and then analyzed using previously-developed methods (Alfarra et al., 2004;Allan et al., 2003a;Allan et al., 2003b;Allan et al., 2004;Jimenez et al., 2003). Calibration

procedures are carried out once per week, including adjustment of the electron multiplier voltage and determination of its gain. Calibration of the overall ionization and detection efficiency (IE) (Allan et al., 2003b;Canagaratna et al., 2007;Jimenez et al., 2003) is performed using a narrow size range selected from a polydisperse ammonium nitrate aerosol (Jayne et al., 2000). Our procedure differs slightly from the conventional AMS calibration (Allan et al., 2003b;Canagaratna et al., 2007;Jimenez et al., 2003), which generates the monodisperse test aerosol using a differential mobility analyzer. We use a polydisperse aerosol together with the sizing capability of the AMS, which is calibrated using size certified polystyrene latex spheres (Jayne et al., 2000). Tests performed in the laboratory prior to installation at PEARL showed that our method gave 10 to 15% lower IE values.

3 Results

The mass concentrations of the chemical species were determined from the measured mass spectra using the fragmentation table as described by (Allan et al., 2004). The lower detection limits for these mass concentrations were estimated as three times the standard deviation of the hourly averages during periods with close to zero concentrations (Allan et al., 2003a;Rupakheti et al., 2005). For a period with relatively low and constant concentrations (September 10 to 11, 2006), this yielded detection limits of 0.02 μg m^{-3} for ammonium, 0.002 μg m^{-3} for nitrate, 0.003 μg m^{-3} for sulfate, and 0.04 μg m^{-3} for organics.

Figures 2 and 3 show time series of AMS mass concentrations of sulfate, total organics, ammonium and nitrate for the aerosol sampled between 2006-08-05 and 2006-10-12, a period with high data coverage (valid data were collected during 97% of the time). The water mass concentration is shown only for particle-bound water (*i.e.* when water correlates obviously with one of the particulate signals). Thus water signals due to varying air humidity levels are ignored (see below). For this period the average mass concentrations for ammonium, nitrate, sulfate, and organics were 0.02 μg m^{-3}, 0.007 μg m^{-3}, 0.115 μg m^{-3} and 0.11 μg m^{-3} respectively. Sulfate was present at concentrations significantly above our previously-defined detection limit. Sulfate occasionally appeared in strong, short-term episodes, three of which are labelled in Figure 2 as 1, 2a and 2b. These will be further analysed in a later section. The organics and nitrate

concentration were clearly above their detection limit most of the time, while most ammonium measurements were approximately at the detection limit. Therefore the ammonium measurement was determined to be too noisy and was not considered in subsequent analyses.

3.1 Regional Atmospheric Chemistry

The data recorded during the first months following the AMS installation give information about the local concentrations that is relevant for the interpretation of the episodes that we will describe later in this paper. During the sampling period, it was found that the absolute mass concentrations of ammonium and nitrate were very low (maxima ~ 0.03-0.05 $\mu g\ m^{-3}$) whereas those of the organic and sulfate components were much higher (maxima ~ 0.5 and 1 $\mu g\ m^{-3}$ respectively). Ammonium nitrate will only form after all the sulfate has been neutralized, so the high sulfate/ammonium ratios indicate that very little ammonium nitrate was present during the sampling period. There is, however, a good correlation between nitrates and organics that persists through the whole dataset. This suggests strongly that the majority of the small nitrate mass concentrations that were observed stem from organic nitrates. This will be discussed further in the next section (3.2). In this context, we note that if inorganic nitrate in the form of ammonium nitrate were present, it is possible that it might be partially re-partitioned from the aerosol to the gas phase during transit through the room temperature inlet following sampling from cold ambient conditions. If this occurred, however, the inorganic component would only be underestimated by less than 10%, (see Sect. 2.2). In view of the discussion at the beginning of this section, however, it is clear that ammonium nitrate aerosol is negligible during the sampling period. Inorganic nitrate may be present in other forms than ammonium nitrate. (Teinilä et al., 2004) found that during their measurements on Svalbard, the nitrate salts were most likely $NaNO_3$ and $Ca(NO_3)_2$, which are non-volatile. They also show additional evidence that nitrate evaporation losses were minimal during their measurements.

(Sirois and Barrie, 1999) report 15 years weekly average measurements of aerosol composition at Alert, 150 km north-east of PEARL. Sulfate was the dominant aerosol component with average concentrations of around 1 $\mu g\ m^{-3}$ in winter and a maximum of 2 $\mu g\ m^{-3}$ in spring. This drops to a minimum of just below 0.1 $\mu g\ m^{-3}$ in July and August, then starts to increase again and reaches about 0.2 $\mu g\ m^{-3}$ in October. Hence, our average sulfate concentrations are very similar to the August-October values of this nearby station. Both nitrate and ammonium concentrations

at Alert were roughly one tenth or less of the sulfate measurements and featured a similar seasonal trend, which was somewhat less pronounced than the sulfate one. Both species have minimum average concentrations in September of around 0.02 μg m^{-3}. This is similar to our average ammonium results and somewhat higher than our nitrate measurements. Other major components at Alert were the refractory species Na, Cl, Al, Ca, and Mg (with concentrations similar to ammonium and nitrate); these cannot be measured with the AMS.

(Sirois and Barrie, 1999) could distinguish two sulfate components, neutralized ammonium sulfate and acidic sulfate, of which the latter was dominant after polar sunrise, presumably due to increased photo-oxidation of SO_2. This is also consistent with our findings of acidic sulfate (see next section, 3.2), with the episodes of very acidic sulfate corresponding to periods of increased SO_2 transport to our site (as we show with Lagrangian analysis, see Sect. 4).

Measurements from Greenland are reported by (Heidam et al., 1993). The semi-weekly average concentrations from four years have seasonal trends similar to those observed at Alert. Sulfate was also in Greenland the predominant component with average concentrations between 0.1 and 0.3 μg m^{-3} during the August-October period, quite similar to our measurements.

3.2 Correlations

Correlations among the sulfate, organics and nitrates for the period shown in Figures 2 and 3 give information about possible common origins for some of these species. The overall correlation coefficient between sulfate and organics for this period is $R^2 = 0.38$. Closer examination of the scatter plot shown in Figure 4 for these two species, however, suggests that aerosols from at least two different sources were sampled. During an episode of high sulfate concentrations that lasted two and a half days (61 h, between 2006-09-01 1:00UTC and 2006-09-03 13:00UTC; shown in blue in Figure 4), the measurements show a high correlation between sulfate and organics ($R^2 = 0.64$), combined with a slowly-varying organic background of around 0.1 μg m^{-3} (*i.e.* the positive intercept in Figure 4). Another subset of measurements with even higher sulfate-to-organics correlation occurred in the data sampled on ten consecutive days between 2006-10-02 and 2006-10-12. These data are shown in green in Figure 4. In this case the correlation coefficient is $R^2 = 0.80$, but there is no significant intercept, suggesting that both particulate organics and sulfate (possibly as precursor gases) arrive from the same source region

in a background-free air mass. We will report the results of Lagrangian studies of these two episodes later in this paper. For other time periods the correlation coefficients are much lower (e.g. R^2 = 0.06 for 2006-09-03 to 2006-09-11). Although there are episodes of both high organic and sulfate particle concentrations during this period, the lack of correlation indicates that they come from different sources and/or geographic regions.

The overall sulfate-nitrate correlation during the same period (2006-08-05 to 2006-10-12) is also weak, with R^2 = 0.24, but the scatter plot shown in Figure 5, reveals periods of higher correlation having similar structures to that of the sulfate-organics episode. These correspond roughly to the two groups of data with higher correlations shown in Figure 4. The first group, which has $SO_4^=$ concentrations above 0.5 μg m^{-3} (episode between 1 September 2006 01:00 UTC and 3 September 2006 13:00 UTC), shows a different trend than points with SO_4 below about 0.4 μg m^{-3}. The second group, between 2 October 2006 and 12 October 2006 (shown in green on the scatter plot in Fig. 5 and having SO_4 concentrations below 0.4 μg m^{-3}) have a higher correlation coefficient, R^2=0.50, than during other periods.

The correlation between nitrate and organics, which is shown in Figure 6, has a higher overall R^2 value of 0.45. This correlation is consistent throughout the entire two months period studied, and no shorter episodes with significantly higher or lower correlation could be identified. This rough correlation between the nitrates and organics in the air at PEARL combined with the absence of natural sources for nitrates near the PEARL laboratory, suggests that both stem from air that is transported to PEARL from low latitude sources where nitrates are prevalent. Since there are no identifiable episodes of very high nitrate concentrations that would indicate localised sources, it is likely that the sources are geographically widespread. This is consistent with agricultural activity as the most likely source, as is the time period, which corresponds to the fall application of nitrate fertilizer. We will comment further on this in the section that reports the Lagrangian calculations.

Relatively low ratios of NO_2^+:NO^+ (the two major nitrate fragments at m/z=46 and m/z=30; this ratio was 0.37 on average) are a further indication that organic nitrate aerosol accounts for most of the measured nitrate (Fry et al., 2009). During calibration of the AMS with ammonium nitrate this ratio is around 1. These organic nitrates are most likely formed during transport and are

responsible for the observed good correlation between nitrate and organics. This would also explain the different sulfate-nitrate trend that we pointed out above for data with sulfate concentrations higher than 0.5 μg m^{-3}. These data were measured during an exceptionally high sulfate episode around 2006-09-02 that was accompanied by a modest increase in the concentration of organics (see Figure 2). The organic aerosol, however, remained correlated to nitrate during the entire episode.

(Bae et al., 2007) suggested determining inorganic nitrate from m/z=46 only by using the 46/30 ratio from calibration and assigning the remaining fraction of m/z=30 to organics. When applying this to our data, the inorganic nitrate as well as the organic part of the AMS nitrate measurement are both still correlated to organics ($R^2 \approx 0.6$). Therefore, our discussions about nitrate are still valid even if we consider this inorganic nitrate only. The average concentration of inorganic nitrate is 0.03 μg m^{-3} (total nitrate from both fragments m/z=30 and 46 is 0.07 μg m^{-3}).

While it is possible that sulfur might have been present in form of ammonium sulfate or bisulfate during periods of low sulfate concentrations, the very low ammonium levels are inconsistent with these compounds being present during episodes with higher sulfur concentrations. This differs from typical urban environments, where most of the sulfur is present as ammonium sulfate and during shorter episodes of increased acidity, ammonium bisulfate is present as well (e.g. Zhang et al., 2005). This suggests that the sulfate aerosol detected during these episodes is probably very highly oxidized and is thus predominantly in the form of sulfuric acid.

3.3 Size Distributions

Mass size distributions of the major chemical species are derived from the AMS measurements in TOF mode (Jimenez et al., 2003). The TOF size distributions shown in Figure 7 are averaged over 2006-09-21 to 2006-10-02, a period that had above average sulfate and organics mass concentrations. The size distributions have been normalized to the mass concentrations determined from measurements in the MS mode (Allan et al., 2003a; Allan et al., 2003b). The sulfate has a distribution between (vacuum aerodynamic) diameters of approximately 200 and 700 nm. The large diameter cutoff may be due in part to the reduced transmission efficiency of the AMS inlet system above this size (Jayne et al., 2000), because Liu et al. (2007) have shown that the transmission efficiency for particles of various compositions drops to about 50% at

around 700 nm. The sulfate distribution is very broad and the shape suggests that it might consist of two modes, one with maximum at approximately 300 nm and one at about 500 nm (or larger). The maximum in the organic aerosol size distribution is at about 350 nm. A weak nitrate mode, similar in shape to the organics, is also evident in this size range. Both contributions from m/z=30 and 46 were considered for this nitrate mode. If only inorganic nitrate (proportional to the m/z=46 fragment) were used, then the TOF data would become too noisy to make any firm statement about the inorganic nitrate mode's location or shape.

Figure 8 shows the size distribution for the short period with exceptionally high sulfate concentration between 2006-09-01 1:00UTC and 2006-09-02 19:00UTC (average sulfate concentration of 0.79 μg m^{-3}). The sulfate mode has a maximum at approximately 500 nm; the maximum in the organic mode is at 450 nm. No significant nitrate was observed during this period. There is, however, a high concentration of particle-bound water (*i.e.* water that was not evaporated from the particle before detection by the AMS). This can be seen in both the time series of total mass concentration and the TOF size distributions. Water that is evaporated from cloud or fog particles in the inlet is seen as fluctuations that have no correlation with the other components. In this case, however, the water signal showed a relatively high correlation with the sulfate (R^2 = 0.46 in MS mode), whereas this R^2 value was 0.07 on the two days prior to this episode. Moreover, the water and sulfate have nearly identical mass size distributions as shown in Figure 8, strongly suggesting that the water was contained in the sulfate particles and was not removed when these particles were heated to room temperature.

During all other periods no identifiable TOF water mode can be distinguished, even on those occasions when the mass concentration of water correlates with sulfate or organics. The absence of a water TOF mode means that little or no moisture remains in the detected particles after passage through the sampling system, indicating that the sampled particles were either dry on entry or contained at most a surface layer of water that evaporates easily. This is consistent with the fact that the temperatures in the vicinity of Eureka were about -12 °C during the sampling period and thus the relative humidity of the air would have been very low after raising its temperature to 20 °C in the inlet. Since the water was not evaporated during the high sulfate episode discussed above, therefore, we conclude that both the sulfate and water come from condensed sulfuric acid. The small amount of organic material present with the water and sulfate

might be from organic aerosols coated with sulfuric acid or from separate organic particles that coincidentally have the same size distribution (Heintzenberg and Leck, 1994). The former, however, seems more likely (Nriagu et al., 1991).

All mass size distributions measured by the AMS during the two months analyzed here extend from about 200 or 300 nm to the upper limit of the AMS at about 700 nm. Although the lower detection limit of the AMS (given at 50% efficiency) is at 80 nm (Liu et al., 2007), none of the measured size distributions show particles below about 200 nm. The absence of ultrafine or Aitken mode particles shows there is no particle formation in the vicinity of PEARL; the arriving particles are aged and thus originate from distant sources. This may be contrasted with AMS studies in urban environments, which usually show two modes: one at 100-200 nm and a larger one between 300 and 800 nm. The smaller mode is normally identified as newly-formed organic particles originating (usually) from motor vehicle emissions, whereas the larger consists of sulfate, nitrate, and oxidized organics (Alfarra et al., 2004;Allan et al., 2003a;Rupakheti et al., 2005). The absence of the smaller mode at PEARL is consistent with results from rural regions, where smaller modes are usually not observed (Alfarra et al., 2004;Rupakheti et al., 2005).

4 Lagrangian Modelling

The correlations described in the last section for some of the episodes are suggestive of common origins, so these episodes were chosen for source identification using the Lagrangian particle dispersion model FLEXPART (Stohl et al., 1998;Stohl and Thomson, 1999). FLEXPART simulates the long-range transport, diffusion, wet and dry deposition, and radioactive decay of tracers released from point, line, area or volume sources. It can be run either in the forward mode to simulate the dispersion of tracers from their sources, or backward in time to determine potential source contributions to a specified receptor. FLEXPART has been extensively validated with data from large-scale tracer experiments in North America and Europe (Stohl et al., 1998) and used in many other atmospheric transport studies. Of relevance to the present high latitude application, FLEXPART was used recently to simulate the transport of pollutant plumes from Russian (Damoah et al., 2004) and Alaskan (Damoah et al., 2006) forest fires. For the simulations reported here, FLEXPART was driven by meteorological data from the Global

Forecast System (GFS) of the National Center for Environmental Prediction using a horizontal resolution of 1° x 1° with 26 pressure levels and a time resolution of 3 hours (analyses at 0, 6, 12, 18 UTC; 3-hour forecasts at 3, 9, 15, 21 UTC).

We ran backward simulations using FLEXPART for the episodes noted in Figure 2 in order to determine the origin of the air arriving at PEARL during those periods. These backward simulations are similar to that described by (Siebert, 2001) and (Stohl et al., 2003). We released 20,000 particles at the PEARL receptor location during the episode periods and simulated their transport backward in time for 20 days, forming a "retroplume". We then computed particle residence times in seconds, normalized by the total number of released particles, in the cells of a 3-D grid with 1° x 1° horizontal resolution and a depth of 500 m above the surface, for each 3 hour transport period.

The residence time in these surface grid boxes is called the source footprint (Flesch et al., 1995) It is proportional to the contribution a source of unit strength located in those grid boxes, would make to the mixing ratio at the receptor. If the absolute contributions from the grid boxes are required in terms of mass concentrations for a particular species, then we multiply the residence times in the grid boxes with the source strength of that species. For the sulfate episodes discussed in the next Section, we used the SO_2 emission for the year 2000 from the Emission Database for Global Atmospheric Research (EDGAR) v3.2 (Olivier et al., 2005) as a proxy for the detected sulfate, on the assumption that the SO_2 would be completely oxidized during transport over the long distances to the receptor.

4.1 Lagrangian Results

As discussed earlier and shown in Figure 2, the sulfate concentrations rose significantly during the period from about 23 August to 8 September – at first gradually, then from about 30 August to 3 September, the AMS recorded sulfate concentrations more than 5 times higher than the average background. Highly variable sulfate concentrations are not unique in the AMS dataset, but the clearly demarcated nature of this example makes it particularly suitable for Lagrangian analysis. The short duration and sudden, high concentrations observed in this episode suggest that it represents the arrival of a "plume" from anthropogenic sources, so we focussed on anthropogenic sulfate emissions during this analysis.

Separate FLEXPART backward simulations were performed for the three sulfate episodes shown in Figure 2 (episodes 1, 2a and 2b) as well as for particles arriving during the clean period from 2006-08-20-00:00z to 2006-08-23-00:00z. Sulfate episode 1 is the relatively small one from 2006-08-30-00:00z to 2006-08-31-00:00z. Sulfate episode 2, which starts at 2006-09-01-00:00z and ends at 2006-09-03-00:00z, has two parts – a larger one from 2006-09-01-00:00z to 2006-09-02-12:00z (episode 2a) and a smaller one from 2006-09-02-12:00z to 2006-09-03-12:00z (episode 2b).

The results from the FLEXPART simulations are shown in Figures 9 – 12. The upper panels in each case show the footprint residence time distributions for particles arriving at PEARL during the respective time periods (normalized by the longest residence time). The upper panel of Figure 9 shows the footprint for the clean air episode; that of Figure 10 shows episode 1 and those of Figures 11 and 12 show episodes 2a and 2b respectively. The sequence of upper panels, beginning with figure 10, shows a large scale circulation pattern that moves strongly southward across eastern North America and the north Atlantic (Figure 10), then continues eastward across northern Eurasia (Figures 11 and 12). During this passage, it crosses regions of anthropogenic activity south of 60^{o}N and picks up SO_2, which is oxidized to $SO_4^{=}$ during transport to the PEARL laboratory. To identify the individual source contributions to the sulfate aerosols detected by the PEARL AMS, we multiply the footprint residence times with the SO_2 emission strengths from the EDGAR inventory. The resulting source contributions are shown in the lower panels of figures 9-12, respectively. For clarity, these panels show only sources with contributions equal to or greater than 10^{-6} ppbv/grid cell.

For the clean air simulation (Figure 9), the retroplume footprint is concentrated at latitudes above 60^{o}N, where anthropogenic activities (and SO_2 emissions) are very low. Consequently, the source map in the lower panel of Figure 9 shows correspondingly low (less than 10^{-6} ppbv/grid cell) sulfate contributions to the mixing ratio at PEARL.

The retroplumes for episodes 1, 2a and 2b, however, extend to lower latitudes, where they encounter anthropogenic SO_2 sources. The upper panel of Figure 10 shows that the longest footprint residence times for episode 1 are in Greenland, but extend southwards over the Atlantic Ocean and parts of eastern Canada down to a latitude of about 40N. A small part of this

footprint also extends over several locations in Russia and Eastern Europe. Combining the EDGAR emission data with this footprint identifies the major source contributions to episode 1, the locations of which are shown in the lower panel of Figure 10. In this case, there are only a few source regions that contribute more than 10^{-6} ppbv/grid cell scattered within the footprint and these are easily identifiable. The locations and most probable identities of the anthropogenic sources responsible for these sulfate emissions are listed in Table 1a. The sources include large cities (Montreal, Moscow), shipping routes in the Atlantic and mining, petroleum and coal producing regions. This shows that the Arctic atmosphere is influenced directly (within 20 days) by a variety of sources at latitudes down to at least 40^{o} N.

By the time episode 2a begins, the footprint region has moved significantly and changed its shape. This reflects both the large scale motion of the upper air and also the turbulence in the lowest meteorological layer in which the footprint is defined. Figure 11 shows that the part of the episode 2a footprint extending over land below 60^{o} N is distributed mainly across northern Eurasia and parts of northern Japan. The source regions that contribute more than 10^{-6} ppbv/grid cell are shown in the lower panel. Again, these are concentrated in a few easily identifiable locations of high emission, which are listed in Table 1b. These are dominated by petroleum production, metals manufacturing and thermal power plants.

The footprint has evolved further by the beginning of episode 2b. At this time, the part that contacts the land surface below 60 N is concentrated largely in eastern Eurasia and the SO_2 sources contributing more than 10^{-6} ppbv/grid cell are found between 50-60^{o} N and 80-100^{o} E (see Figure 12 and Table 1c). In this case, heavy industry, petroleum refining, chemical and cement processing appear to dominate the anthropogenic SO_2 sources.

5 Conclusions

We have described the installation of an AMS at the PEARL observatory in the Canadian high Arctic and discussed several technical aspects that ensure the integrity of particles sampled from the very cold and harsh environment at the laboratory. The uniquely remote location of the laboratory at 80^{o} N and an altitude of 610 m above sea level (in the free troposphere) make it an ideal site to study the long range transport of pollutants into the Arctic.

Since its installation, the AMS has been providing a record of the mass concentrations as well as the chemical composition and size distribution of ambient aerosol at the PEARL site. In this paper, we have reported the compositions and size distributions of the aerosols measured during selected episodes as well as during periods in which normal background was observed. We have found that some of the components have common origins, based on their high temporal correlations during certain periods.

We have also used Lagrangian modelling to examine three selected episodes during which unusually high sulfate concentrations were observed. The temporal profiles of these suggest anthropogenic origins. In all cases, these coincided with the arrival of air that had contacted the surface at latitudes below about 60^{o} N. Most of these lower-latitude footprints were on land, but sulfate emissions from shipping in the Atlantic were also detected. Land source regions were found in north-eastern North America and in a broad area of northern Eurasia, principally in Russia. These Lagrangian results demonstrate that there is direct transport of polluted air into the high Arctic (up to 80^{o}N) from latitudes down to 40^{o}N on a time scale of 2-3 weeks. The polluted air originates in a wide variety of industrial, resource extraction and petroleum-related activity as well as from large population centres. The quantification of this transport is important not only to our understanding of the sources of Arctic pollution, but also for international discussions aimed at its abatement. In future publications, we hope to assess the sources for other kinds of aerosols, including organics, to further elucidate the transport of these materials into the Arctic.

6 Acknowledgements

We are grateful for the financial assistance of the Canada Foundation for Climate and Atmospheric Studies (CFCAS) and for helpful discussions with Dr. John Jayne, Aerodyne Inc.

7 Figure captions:

Figure 1

A 30° radial section is used to model the flow through the inlet assembly with CFD. Air at -40°C and 1 μm diameter particles (density of 1000 kg m^{-3}) are introduced through the opening at the bottom of the inlet. The outer surface and the inlet pipe in the center (ending in a funnel at the top) are heated to 20°C. Trajectories of the 1 μm particles are depicted as grey lines.

Figure 2

Time series of AMS mass concentrations of sulfate, total organics, ammonium and nitrate for the aerosol sampled between 2006-08-05 and 2006-09-11. Four periods were selected for subsequent analysis. These are labelled "Clean" (indicating low levels of all detected species) and 1, 2a and 2b, during which high sulfate levels were detected. See Figures 9-12 for Lagrangian modelling of these periods.

Figure 3

Time series of AMS mass concentrations of sulfate, total organics, ammonium and nitrate for the aerosol sampled between 2006-09-13, 00:00 UTC and 2006-10-13, 00:00 UTC

Figure 4

Scatter plot of organics and sulfate concentrations showing data between 2006-08-05 and 2006-10-12. Two groups with exceptionally high correlations are indicated with blue and green points. The remaining data are shown as black points.

Figure 5

Scatter plot of nitrate and sulfate concentrations showing data between 2006-08-05 and 2006-10-12. The overall correlation is weak with R^2 of 0.24. One group with high correlation is indicated with green points. The remaining data are shown as black points.

Figure 6

Scatter plot of organics and nitrate concentrations showing data between 2006-08-05 and 2006-10-12. The consistent overall correlation has an R^2 value of 0.45.

Figure 7

Mass size distributions averaged over the period from 2006-09-21 to 2006-10-02 having above average sulfate and organics mass concentrations.

Figure 8

Mass size distributions for an episode with exceptionally high sulfate concentrations (2006-09-01-01, 00:00 UTC to 2006-09-02, 19:00 UTC). During this episode particle-bound water was detected with a size distribution similar to the sulfate size distribution.

Figure 9

The top panel shows the footprint residence time distribution for particles arriving at the receptor during the "clean" period from 2006-08-20, 00:00 UTC to 2006-08-23, 00:00 UTC. The values are expressed as a percentage of the maximum residence time (17.7 s) in each grid cell. The corresponding source contributions per grid cell to the mixing ratio at the receptor are shown in the bottom panel.

Figure 10

Similar to Fig. 9 but for particles arriving at the receptor from 2006-08-30, 00:00 UTC to 2006-08-31, 00:00 UTC. Maximum residence time: 8.2 s.

Figure 11

Similar to Fig. 9, but for particles arriving at the receptor between 2006-09-01, 00:00 UTC and 2006-09-02, 12:00 UTC. Maximum residence time: 16.3 s.

Figure 12

Similar to Fig. 9, but for particles arriving at the receptor between 2006-09-02, 12:00 UTC and 2006-09-03, 12:00 UTC. Maximum residence time: 6.5 s.

629 References

630

631 Alfarra, M. R., H. Coe, J. D. Allan, K. N. Bower, H. Boudries, M. R. Canagaratna, J. L. Jimenez,
632 J. T. Jayne, A. A. Garforth, S. M. Li and D. R. Worsnop, Characterization of urban and
633 rural organic particulate in the lower Fraser valley using two aerodyne aerosol mass
634 spectrometers, *Atmospheric Environment, 38*(34), 5745-5758, 2004.

635 Allan, J. D., M. R. Alfarra, K. N. Bower, P. I. Williams, M. W. Gallagher, J. L. Jimenez, A. G.
636 McDonald, E. Nemitz, M. R. Canagaratna, J. T. Jayne, H. Coe and D. R. Worsnop,
637 Quantitative sampling using an Aerodyne aerosol mass spectrometer - 2. Measurements
638 of fine particulate chemical composition in two U.K. cities, *Journal of Geophysical*
639 *Research-Atmospheres, 108*(D3), 4091, 2003a.

640 Allan, J. D., A. E. Delia, H. Coe, K. N. Bower, M. R. Alfarra, J. L. Jimenez, A. M. Middlebrook,
641 F. Drewnick, T. B. Onasch, M. R. Canagaratna, J. T. Jayne and D. R. Worsnop, A
642 generalised method for the extraction of chemically resolved mass spectra from aerodyne
643 aerosol mass spectrometer data, *Journal of Aerosol Science, 35*(7), 909-922, 2004.

644 Allan, J. D., J. L. Jimenez, P. I. Williams, M. R. Alfarra, K. N. Bower, J. T. Jayne, H. Coe and D.
645 R. Worsnop, Quantitative sampling using an Aerodyne aerosol mass spectrometer - 1.
646 Techniques of data interpretation and error analysis, *Journal of Geophysical Research-*
647 *Atmospheres, 108*(D3), 4090, 2003b.

648 AMAP, AMAP Assessment 2002: The Influence of Global Change on Contaminant Pathways to,
649 within, and from the Arctic, 2003.

650 Bae, M. S., J. J. Schwab, Q. Zhang, O. Hogrefe, K. L. Demerjian, S. Weimer, K. Rhoads, D.
651 Orsini, P. Venkatachari and P. K. Hopke, Interference of organic signals in highly time
652 resolved nitrate measurements by low mass resolution aerosol mass spectrometry,
653 *Journal of Geophysical Research-Atmospheres, 112*, 2007.

654 Bailey, R., L. A. Barrie, C. J. Halsall, P. Fellin and D. C. G. Muir, Atmospheric organochlorine
655 pesticides in the western Canadian Arctic: Evidence of transpacific transport, *Journal of*
656 *Geophysical Research-Atmospheres, 105*(D9), 11805-11811, 2000.

657 Barrie, L. A., R. Staebler, D. Toom, B. Georgi, G. Denhartog, S. Landsberger and D. Wu, Arctic
658 Aerosol Size-Segregated Chemical Observations in Relation to Ozone Depletion During
659 Polar Sunrise Experiment 1992, *Journal of Geophysical Research-Atmospheres,*
660 *99*(D12), 25439-25451, 1994.

661 Bergin, M. H., J. A. Ogren, S. E. Schwartz and L. M. McInnes, Evaporation of ammonium
662 nitrate aerosol in a heated nephelometer: Implications for field measurements,
663 *Environmental Science & Technology, 31*(10), 2878-2883, 1997.

664 Canagaratna, M. R., J. T. Jayne, J. L. Jimenez, J. D. Allan, M. R. Alfarra, Q. Zhang, T. B.
665 Onasch, F. Drewnick, H. Coe, A. Middlebrook, A. Delia, L. R. Williams, A. M.
666 Trimborn, M. J. Northway, P. F. DeCarlo, C. E. Kolb, P. Davidovits and D. R. Worsnop,
667 Chemical and microphysical characterization of ambient aerosols with the aerodyne
668 aerosol mass spectrometer, *Mass Spectrometry Reviews, 26*(2), 185-222, 2007.

669 Covert, D. S. and J. Heintzenberg, Size Distributions and Chemical-Properties of Aerosol at Ny
670 Ålesund, Svalbard, *Atmospheric Environment Part A-General Topics, 27*(17-18), 2989-
671 2997, 1993.

672 Damoah, R., N. Spichtinger, C. Forster, P. James, I. Mattis, U. Wandinger, S. Beirle, T. Wagner
673 and A. Stohl, Around the world in 17 days - hemispheric-scale transport of forest fire
674 smoke from Russia in May 2003, *Atmospheric Chemistry and Physics, 4*, 1311-1321,
675 2004.

676 Damoah, R., N. Spichtinger, R. Servranckx, M. Fromm, E. W. Eloranta, I. A. Razenkov, P.
677 James, M. Shulski, C. Forster and A. Stohl, A case study of pyro-convection using
678 transport model and remote sensing data, *Atmospheric Chemistry and Physics, 6*, 173-
679 185, 2006.

680 Flesch, T. K., J. D. Wilson and E. Yee, Backward-Time Lagrangian stochastic dispersion
681 models and their application to estimate gaseous emissions, *Journal of Applied*
682 *Meteorology, 34*, 1320-1332, 1995.

683 Fry, J. L., A. Kiendler-Scharr, A. W. Rollins, P. J. Wooldridge, S. S. Brown, H. Fuchs, W. Dubé,
684 A. Mensah, M. Dal Maso, R. Tillmann, H.-P. Dorn, T. Brauers and R. C. Cohen,
685 Organic nitrate and secondary organic aerosol yield from NO_3 oxidation of ß-pinene
686 evaluated using a gas-phase kinetics/aerosol partitioning model, *Atmospheric Chemistry*
687 *and Physics, 9*, 1431-1449, 2009.

688 Gormley, P. G. and M. Kennedy, Diffusion from a stream flowing through a cylindrical tube,
689 *Proceedings of the Royal Irish Academy, A52*, 163-169, 1949.

690 Halsall, C. J., R. Bailey, G. A. Stern, L. A. Barrie, P. Fellin, D. C. G. Muir, B. Rosenberg, F. Y.
691 Rovinsky, E. Y. Kononov and B. Pastukhov, Multi-year observations of organohalogen
692 pesticides in the Arctic atmosphere, *Environmental Pollution, 102*(1), 51-62, 1998.

693 Halsall, C. J., L. A. Barrie, P. Fellin, D. C. G. Muir, B. N. Billeck, L. Lockhart, F. Y. Rovinsky,
694 E. Y. Kononov and B. Pastukhov, Spatial and temporal variation of polycyclic aromatic
695 hydrocarbons in the Arctic atmosphere, *Environmental Science & Technology, 31*(12),
696 3593-3599, 1997.

697 Heidam, N. Z., P. Wahlin and K. Kemp, Arctic Aerosols in Greenland, *Atmospheric*
698 *Environment Part A-General Topics, 27*(17-18), 3029-3036, 1993.

699 Heintzenberg, J., Arctic Haze - Air-Pollution in Polar-Regions, *Ambio, 18*(1), 50-55, 1989.

Heintzenberg, J. and C. Leck, Seasonal-Variation of the Atmospheric Aerosol Near the Top of the Marine Boundary-Layer Over Spitsbergen Related to the Arctic Sulfur Cycle, *Tellus Series B-Chemical and Physical Meteorology, 46*(1), 52-67, 1994.

Hillamo, R., V. M. Kerminen, M. Aurela, T. Makela, W. Maenhaut and C. Leck, Modal structure of chemical mass size distribution in the high Arctic aerosol, *Journal of Geophysical Research-Atmospheres, 106*(D21), 27555-27571, 2001.

Hinds, W. C., Aerosol Technology: Properties, Behavior, and Measurement of Airborne Particles, John Wiley & Sons, New York, 1999.

Hoff, R. M., W. R. Leaitch, P. Fellin and L. A. Barrie, Mass Size Distributions of Chemical-Constituents of the Winter Arctic Aerosol, *Journal of Geophysical Research-Oceans and Atmospheres, 88*(NC15), 947-956, 1983.

Hung, H., P. Blanchard, C. J. Halsall, T. F. Bidleman, G. A. Stern, P. Fellin, D. C. G. Muir, L. A. Barrie, L. M. Jantunen, P. A. Helm, J. Ma and A. Konoplev, Temporal and spatial variabilities of atmospheric polychlorinated biphenyls (PCBs), organochlorine (OC) pesticides and polycyclic aromatic hydrocarbons (PAHs) in the Canadian Arctic: Results from a decade of monitoring, *Science of the Total Environment, 342*(1-3), 119-144, 2005.

Incropera, F. P. and D. P. DeWitt, Fundamentals of Heat and Mass Transfer, Wiley, New York, 1999.

Jayne, J. T., D. C. Leard, X. F. Zhang, P. Davidovits, K. A. Smith, C. E. Kolb and D. R. Worsnop, Development of an aerosol mass spectrometer for size and composition analysis of submicron particles, *Aerosol Science and Technology, 33*(1-2), 49-70, 2000.

Jimenez, J. L., J. T. Jayne, Q. Shi, C. E. Kolb, D. R. Worsnop, I. Yourshaw, J. H. Seinfeld, R. C. Flagan, X. F. Zhang, K. A. Smith, J. W. Morris and P. Davidovits, Ambient aerosol sampling using the Aerodyne Aerosol Mass Spectrometer, *Journal of Geophysical Research-Atmospheres, 108*(D7), 2003.

Lammel, G., A. M. Sehili, T. C. Bond, J. Feichter and H. Grassl, Gas/particle partitioning and global distribution of polycyclic aromatic hydrocarbons - A modelling approach, *Chemosphere, 76*(1), 98-106, 2009.

Liu, P. S. K., R. Deng, K. A. Smith, L. R. Williams, J. T. Jayne, M. R. Canagaratna, K. Moore, T. B. Onasch, D. R. Worsnop and T. Deshler, Transmission efficiency of an aerodynamic focusing lens system: Comparison of model calculations and laboratory measurements for the Aerodyne Aerosol Mass Spectrometer, *Aerosol Science and Technology, 41*(8), 721-733, 2007.

Narukawa, M., K. Kawamura, S. M. Li and J. W. Bottenheim, Dicarboxylic acids in the Arctic aerosols and snowpacks collected during ALERT 2000, *Atmospheric Environment, 36*(15-16), 2491-2499, 2002.

736 Nriagu, J. O., R. D. Coker and L. A. Barrie, Origin of Sulfur in Canadian Arctic Haze from
737 Isotope Measurements, *Nature, 349*(6305), 142-145, 1991.

738 Nyeki, S., G. Coulson, I. Colbeck, K. Eleftheriadis, U. Baltensperger and H. J. Beine, Overview
739 of aerosol microphysics at Arctic sunrise: measurements during the NICE renoxification
740 study, *Tellus Series B-Chemical and Physical Meteorology, 57*(1), 40-50, 2005.

741 Oehme, M., Further Evidence for Long-Range Air Transport of Polychlorinated Aromates and
742 Pesticides - North-America and Eurasia to the Arctic, *Ambio, 20*(7), 293-297, 1991.

743 Oehme, M. and B. Ottar, The Long-Range Transport of Polychlorinated Hydrocarbons to the
744 Arctic, *Geophys. Res. Lett., 11*(11), 1133-1136, 1984.

745 Olivier, J. G. J., J. A. Van Ardenne, F. Dentner, L. Ganzeveld and J. A. H. Peters, Recent trends
746 in global greenhouse gas emissions regional trends and spatial distribution of key
747 sources, in *Non-CO2 Greenhouse Gases (NCGG4)*, edited by A. van Amstel, pp. 325-
748 330, Millpress, Rotterdam, 2005.

749 Pacyna, J. M., The Origin of Arctic Air-Pollutants - Lessons Learned and Future-Research,
750 *Science of the Total Environment, 161*, 39-53, 1995.

751 Polissar, A. V., P. K. Hopke and J. M. Harris, Source regions for atmospheric aerosol measured
752 at Barrow, Alaska, *Environmental Science & Technology, 35*(21), 4214-4226, 2001.

753 Ricard, V., J. L. Jaffrezo, V. M. Kerminen, R. E. Hillamo, K. Teinila and W. Maenhaut, Size
754 distributions and modal parameters of aerosol constituents in northern Finland during the
755 European Arctic Aerosol Study, *Journal of Geophysical Research-Atmospheres,*
756 *107*(D14), 2002.

757 Rupakheti, M., W. R. Leaitch, U. Lohmann, K. Hayden, P. Brickell, G. Lu, S. M. Li, D. Toom-
758 Sauntry, J. W. Bottenheim, J. R. Brook, R. Vet, J. T. Jayne and D. R. Worsnop, An
759 intensive study of the size and composition of submicron atmospheric aerosols at a rural
760 site in Ontario, Canada, *Aerosol Science and Technology, 39*(8), 722-736, 2005.

761 Saarikoski, S., H. Timonen, K. Saarnio, M. Aurela, L. Jarvi, P. Keronen, V. M. Kerminen and R.
762 Hillamo, Sources of organic carbon in fine particulate matter in northern European urban
763 air, *Atmospheric Chemistry and Physics, 8*(20), 6281-6295, 2008.

764 Sehili, A. M. and G. Lammel, Global fate and distribution of polycyclic aromatic hydrocarbons
765 emitted from Europe and Russia, *Atmospheric Environment, 41*(37), 8301-8315, 2007.

766 Siebert, P., Inverse modeling with a Lagrangian particle dispersion model, Application to point
767 releases over limited time intervals, paper presented at *Air pollution Modeling and its*
768 *Application XI; Proceedings of ITM Boulder*, 2001.

769 Sirois, A. and L. A. Barrie, Arctic lower tropospheric aerosol trends and composition at Alert,
770 Canada: 1980-1995, *Journal of Geophysical Research-Atmospheres, 104*(D9), 11599-
771 11618, 1999.

772 Staebler, R., D. Toom-Sauntry, L. Barrie, U. Langendorfer, E. Lehrer, S. M. Li and H. Dryfhout-
773 Clark, Physical and chemical characteristics of aerosols at Spitsbergen in the spring of
774 1996, *Journal of Geophysical Research-Atmospheres, 104*(D5), 5515-5529, 1999.

775 Stelson, A. W. and J. H. Seinfeld, Relative humidity and temperature dependence of the
776 ammonium nitrate dissociation constant, *Atmospheric Environment, 41*(Supplement),
777 126-135, 2007.

778 Stohl, A., C. Forster, S. Eckhardt, N. Spichtinger, H. Huntrieser, J. Heland, H. Schlager, S.
779 Wilhelm, F. Arnold and O. Cooper, A backward modeling study of intercontinental
780 pollution transport using aircraft measurements, *Journal of Geophysical Research-*
781 *Atmospheres, 108*(D12), 2003.

782 Stohl, A., M. Hittenberger and G. Wotawa, Validation of the Lagrangian particle dispersion
783 model FLEXPART against large-scale tracer experiment data, *Atmospheric Environment,*
784 *32*(24), 4245-4264, 1998.

785 Stohl, A. and D. J. Thomson, A density correction for Lagrangian particle dispersion models,
786 *Boundary-Layer Meteorology, 90*(1), 155-167, 1999.

787 Ström, J., J. Umegard, K. Torseth, P. Tunved, H. C. Hansson, K. Holmen, V. Wismann, A.
788 Herber and G. Konig-Langlo, One year of particle size distribution and aerosol chemical
789 composition measurements at the Zeppelin Station, Svalbard, March 2000-March 2001,
790 *Physics and Chemistry of the Earth, 28*(28-32), 1181-1190, 2003.

791 Teinilä, K., R. Hillamo, V. M. Kerminen and H. J. Beine, Chemistry and modal parameters of
792 major ionic aerosol components during the NICE campaigns at two altitudes,
793 *Atmospheric Environment, 38*(10), 1481-1490, 2004.

794 Teinilä, K., R. Hillamo, V. M. Kerminen and H. J. Beine, Aerosol chemistry during the NICE
795 dark and light campaigns, *Atmospheric Environment, 37*(4), 563-575, 2003.

796 US EIA, Russian Oil Production (on line), *U. S. Energy Information Administration*, 2009.

797 Xie, Y. L., P. K. Hopke, P. Paatero, L. A. Barrie and S. M. Li, Locations and preferred pathways
798 of possible sources of Arctic aerosol, *Atmospheric Environment, 33*(14), 2229-2239,
799 1999.

800 Zhang, Q., M. R. Canagaratna, J. T. Jayne, D. R. Worsnop and J. L. Jimenez, Time- and size-
801 resolved chemical composition of submicron particles in Pittsburgh: Implications for
802 aerosol sources and processes, *Journal of Geophysical Research-Atmospheres, 110*(D7),
803 2005.

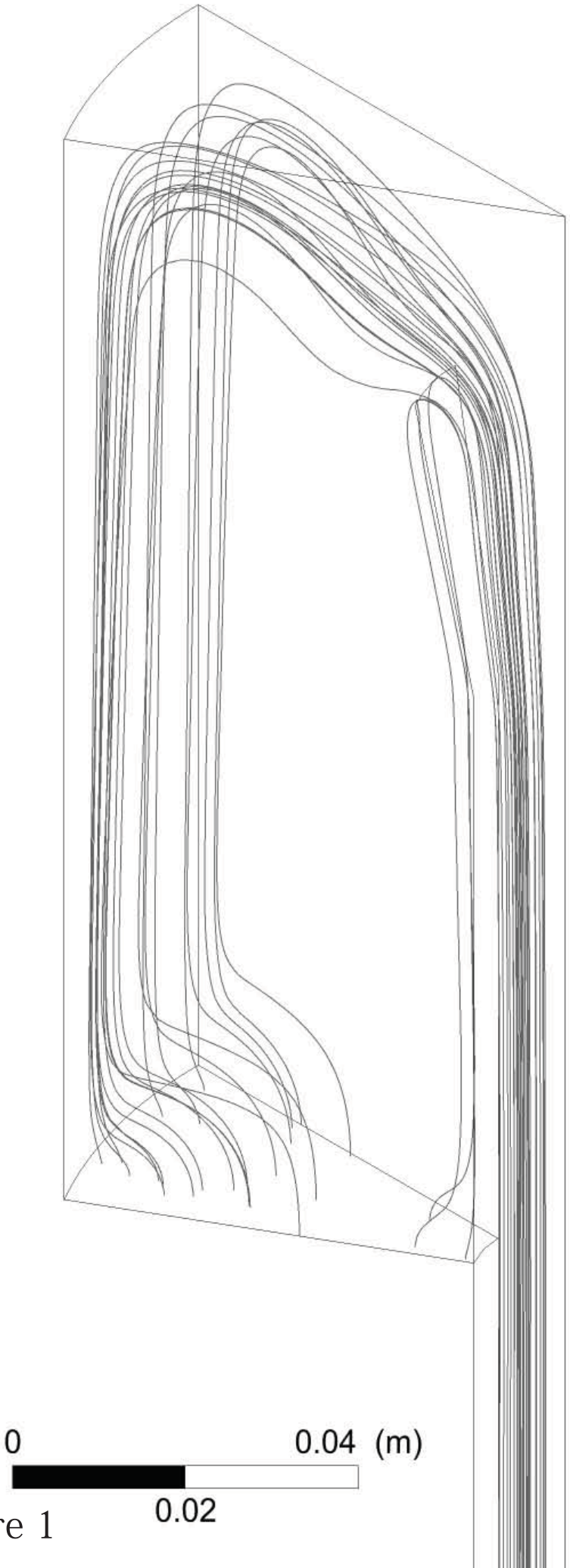

Figure 1

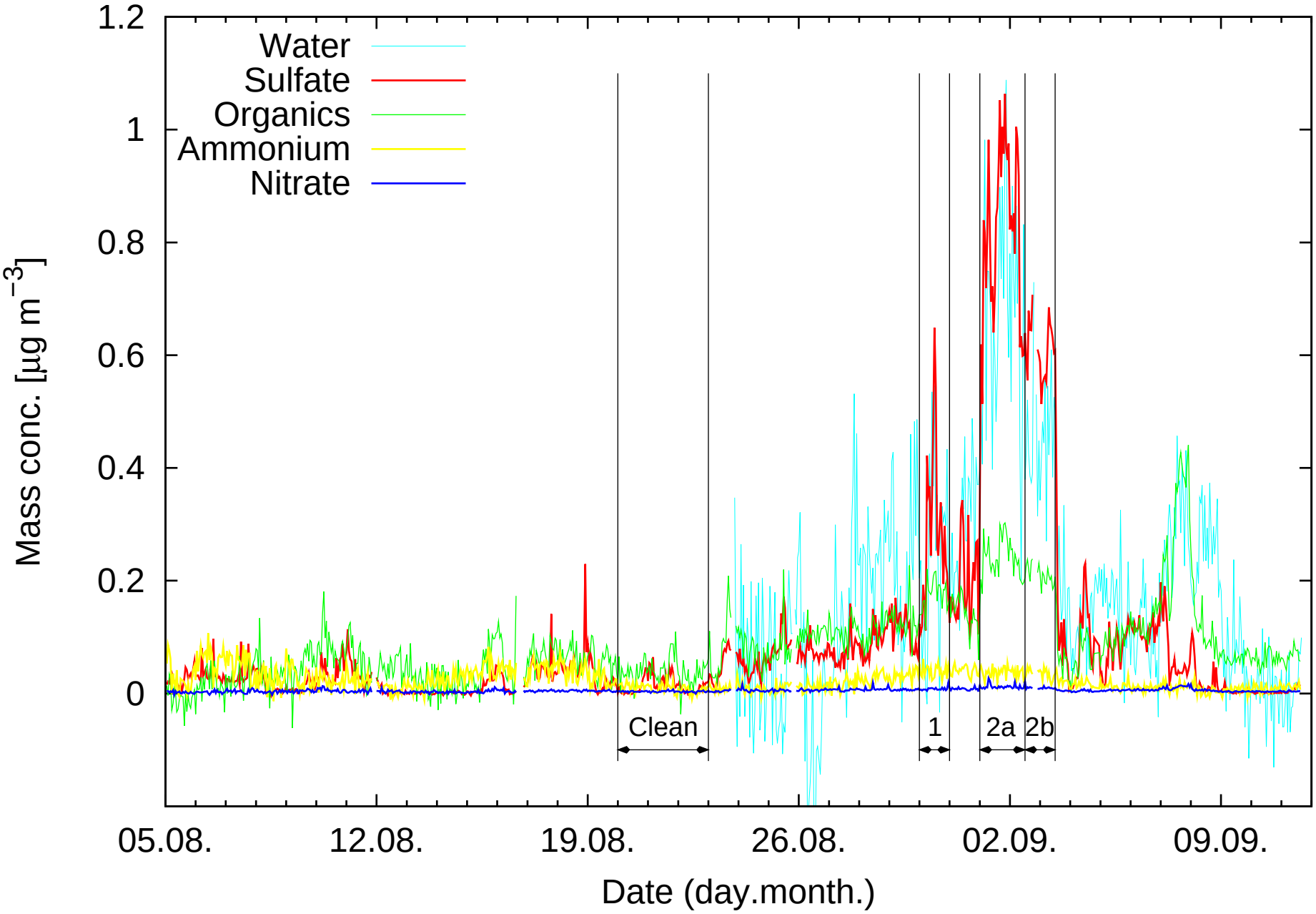
Water
Sulfate
Organics
Ammonium
Nitrate
Mass conc. [µg m^{-3}]
1.2
1
0.8
0.6
0.4
0.2
0
Clean
1
2a
2b
05.08.
12.08.
19.08.
26.08.
02.09.
09.09.
Date (day.month.)

Figure 2

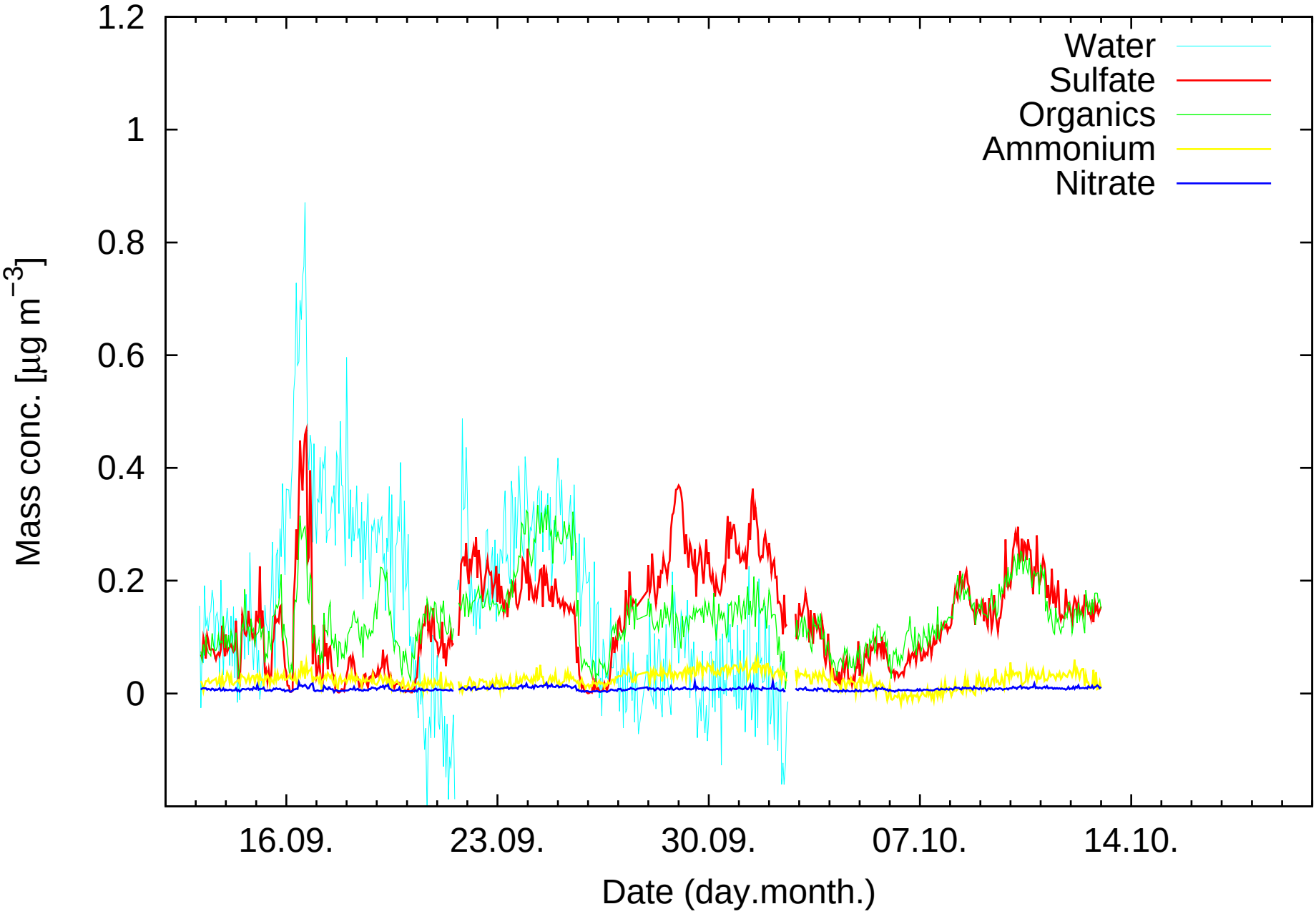
Water
Sulfate
Organics
Ammonium
Nitrate
Mass conc. [µg m^{-3}]
1.2
1
0.8
0.6
0.4
0.2
0
16.09.
23.09.
30.09.
07.10.
14.10.
Date (day.month.)

Figure 3

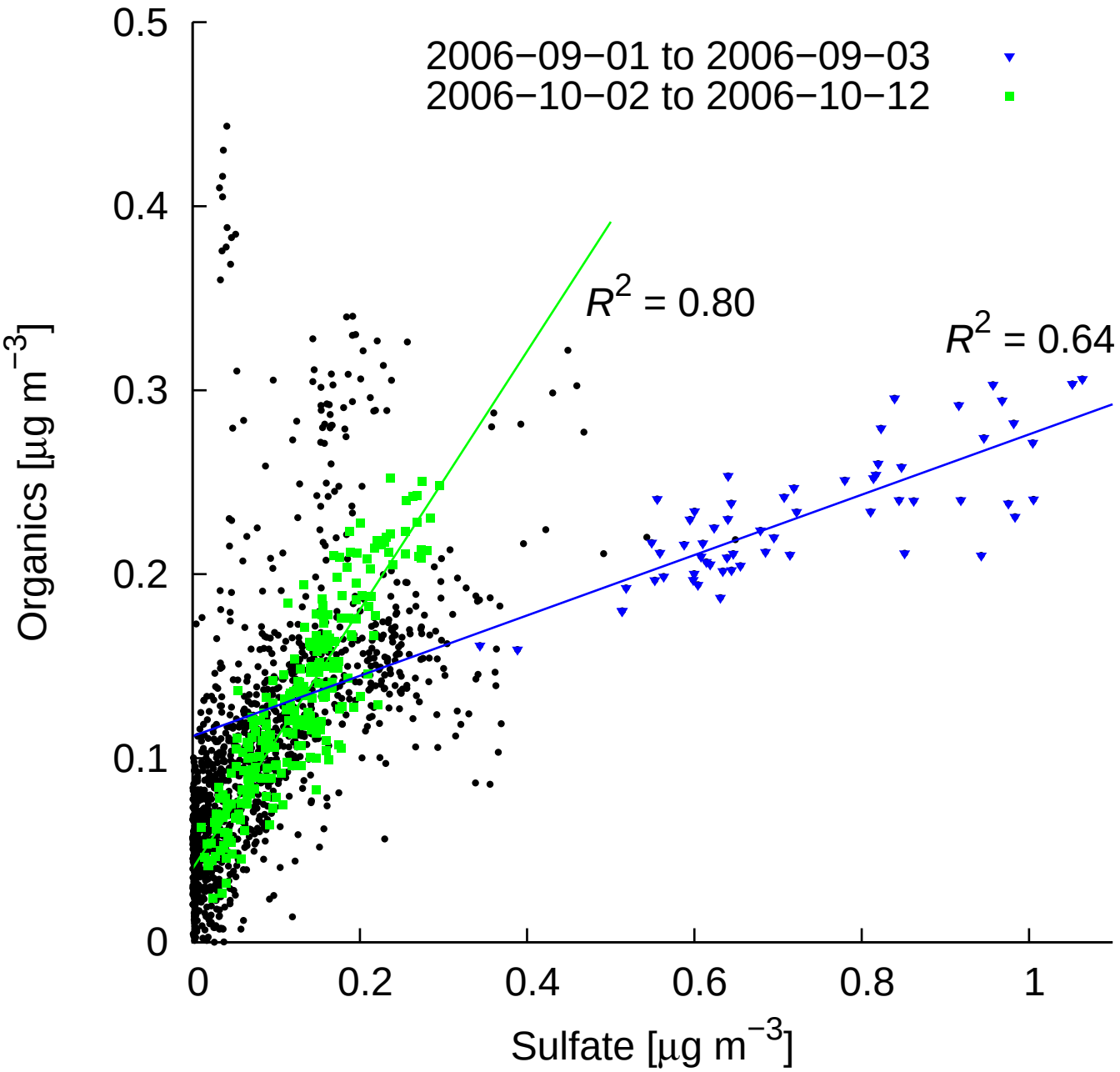
2006−09−01 to 2006−09−03
2006−10−02 to 2006−10−12
R^2 = 0.80
R^2 = 0.64
Organics [µg m^{-3}]
Sulfate [µg m^{-3}]
0
0.1
0.2
0.3
0.4
0.5
0
0.2
0.4
0.6
0.8
1

Figure 4

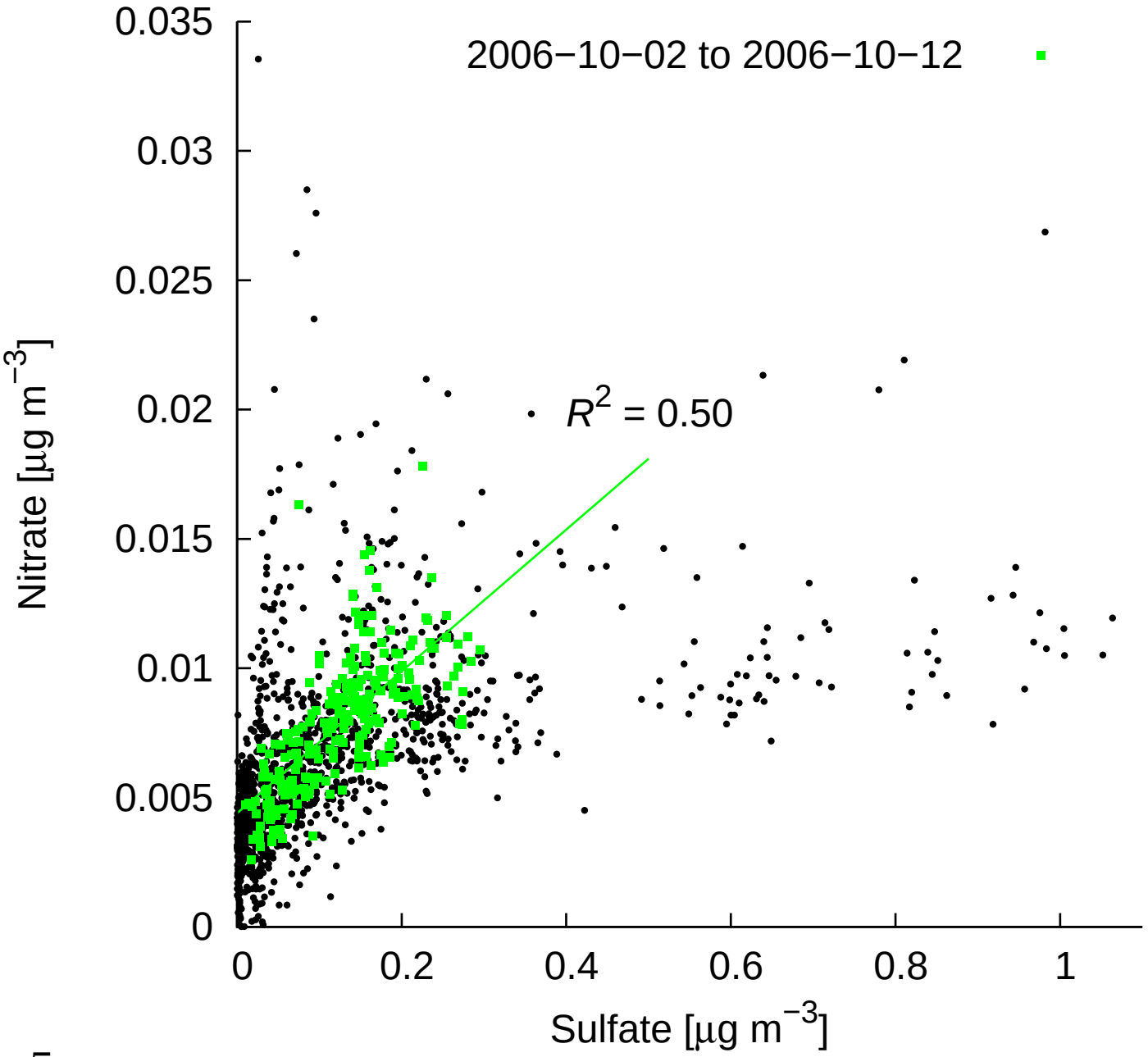
2006−10−02 to 2006−10−12
R^2 = 0.50
Nitrate [µg m^{-3}]
Sulfate [µg m^{-3}]
0.035
0.03
0.025
0.02
0.015
0.01
0.005
0
0
0.2
0.4
0.6
0.8
1

Figure 5

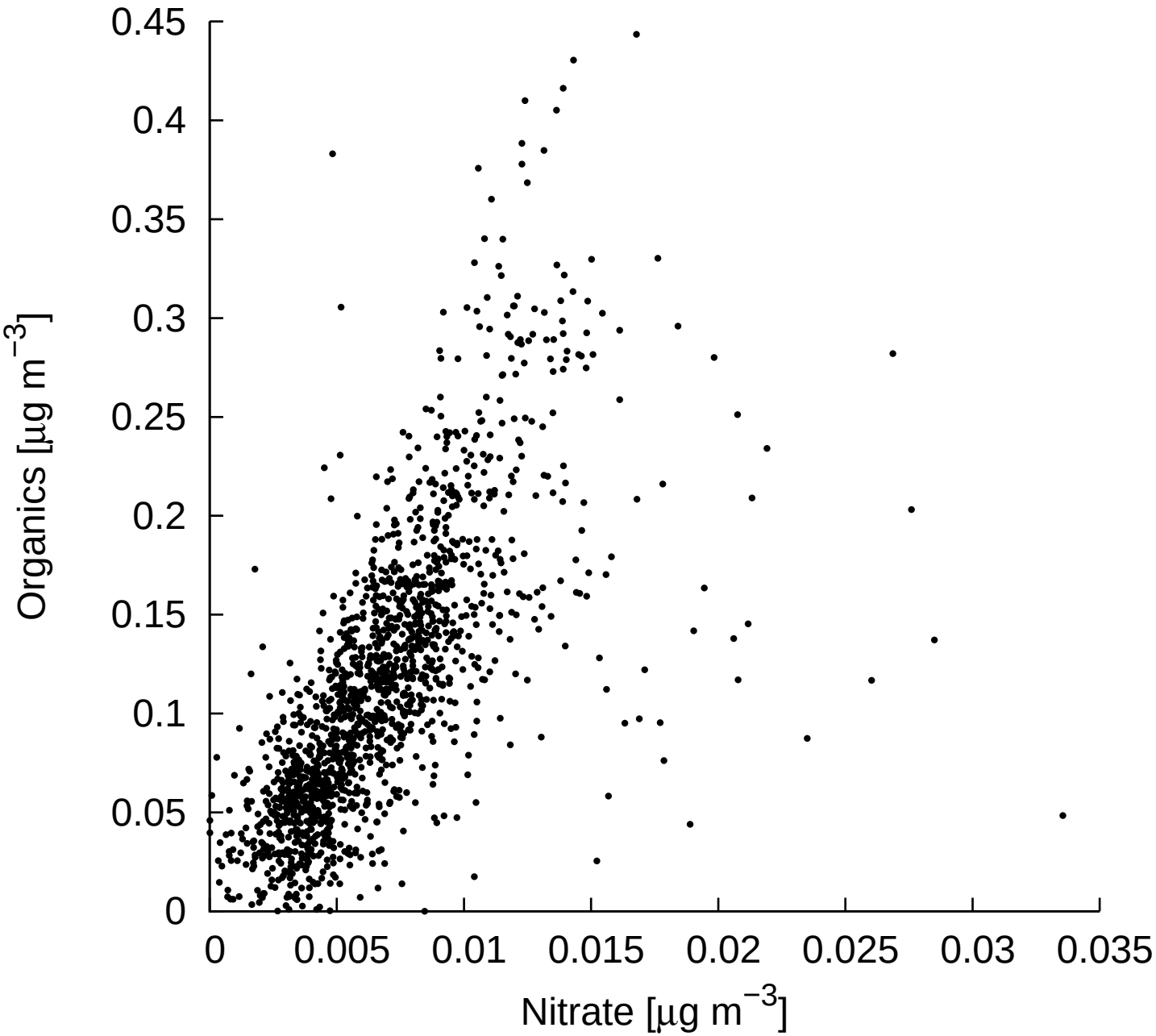
0.45
0.4
0.35
0.3
0.25
0.2
0.15
0.1
0.05
0
Organics [µg m^{-3}]
0
0.005
0.01
0.015
0.02
0.025
0.03
0.035
Nitrate [µg m^{-3}]

Figure 6

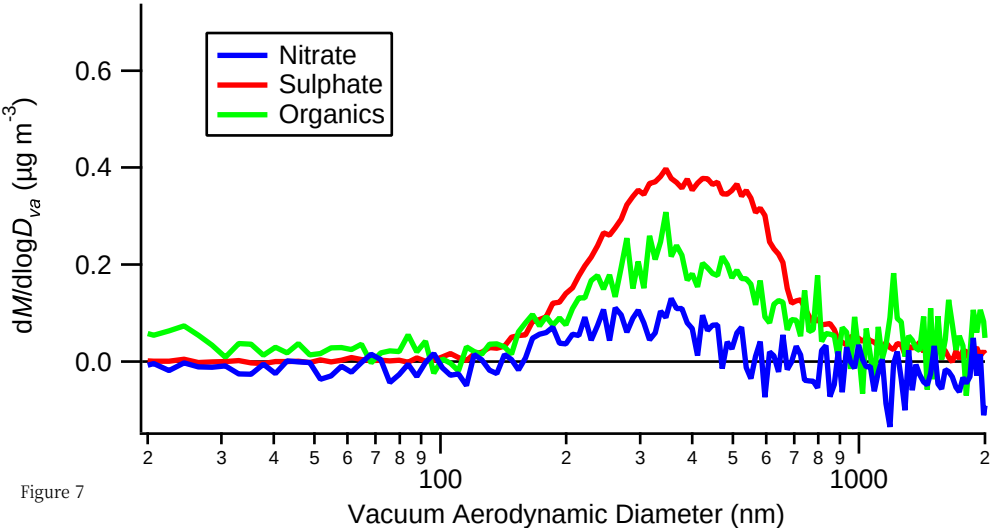
Nitrate
Sulphate
Organics
0.6
0.4
0.2
0.0
dM/dlogD_va (µg m^-3)
2
3
4
5
6
7
8
9
100
2
3
4
5
6
7
8
9
1000
2
Vacuum Aerodynamic Diameter (nm)

Figure 7

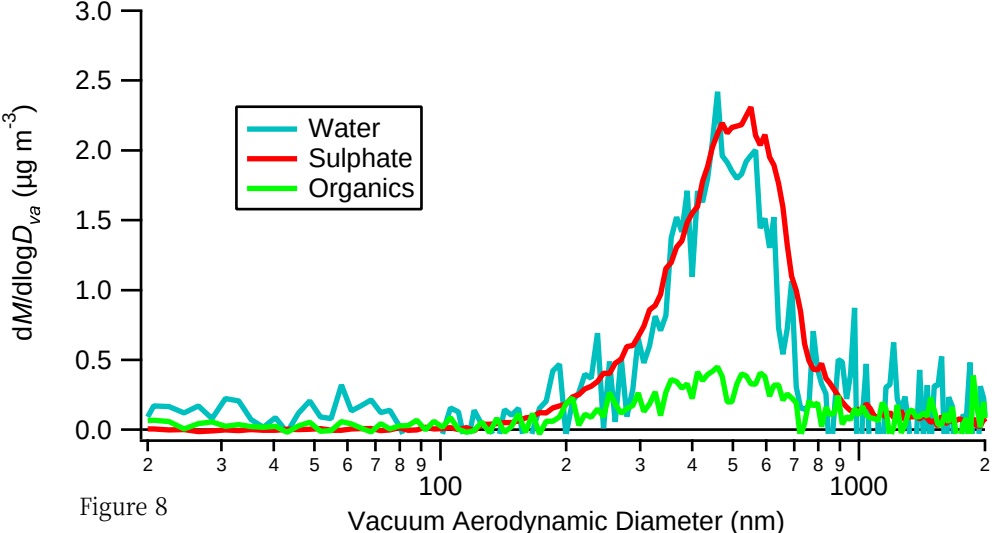
3.0
2.5
2.0
1.5
1.0
0.5
0.0
dM/dlogDva (µg m-3)
Water
Sulphate
Organics
2
3
4
5
6
7
8
9
100
2
3
4
5
6
7
8
9
1000
2
Vacuum Aerodynamic Diameter (nm)

Figure 8

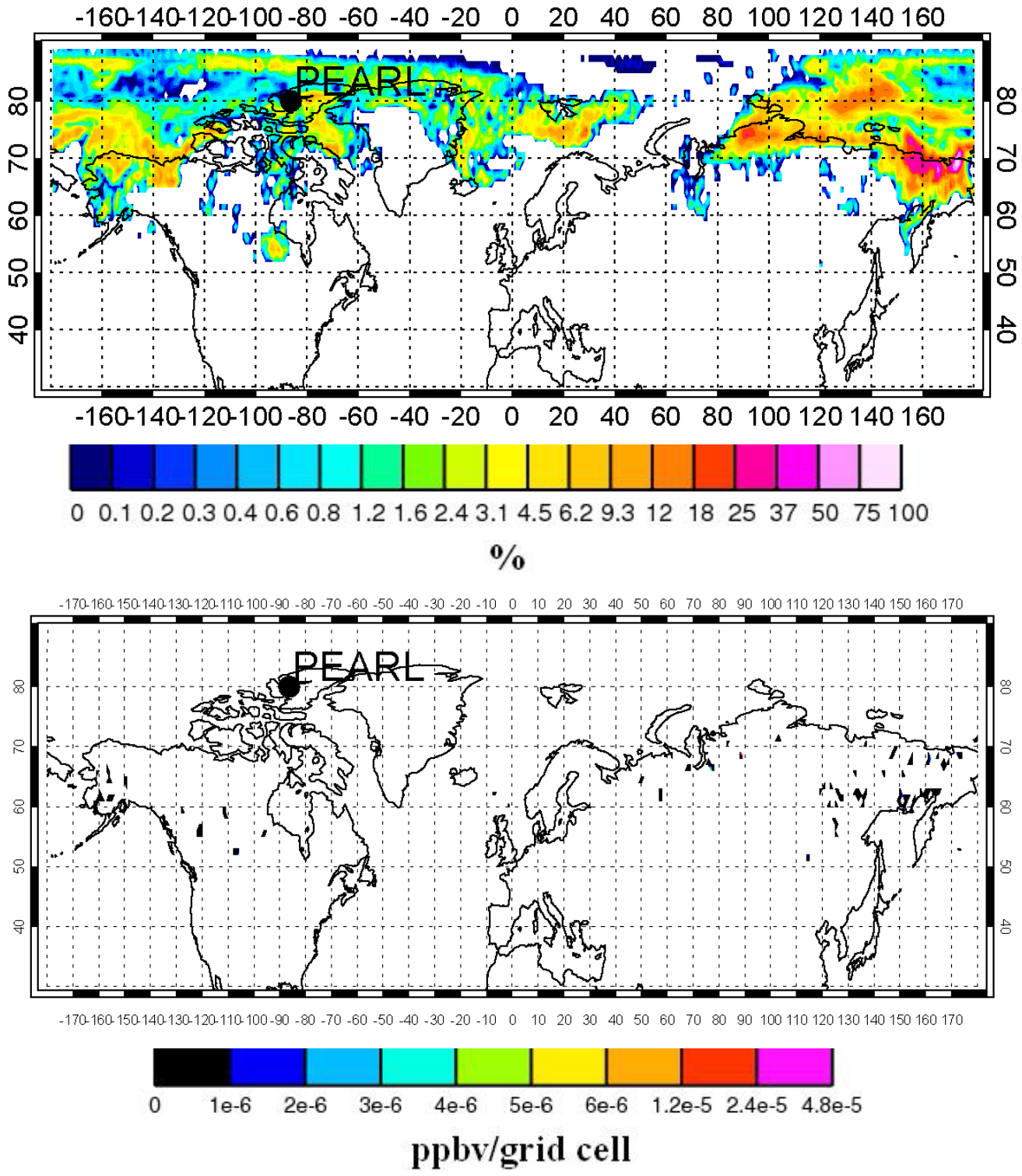
-160 -140 -120 -100 -80 -60 -40 -20 0 20 40 60 80 100 120 140 160
PEARL
80 70 60 50 40
0 0.1 0.2 0.3 0.4 0.6 0.8 1.2 1.6 2.4 3.1 4.5 6.2 9.3 12 18 25 37 50 75 100
%
-170 -160 -150 -140 -130 -120 -110 -100 -90 -80 -70 -60 -50 -40 -30 -20 -10 0 10 20 30 40 50 60 70 80 90 100 110 120 130 140 150 160 170
PEARL
80 70 60 50 40
0 1e-6 2e-6 3e-6 4e-6 5e-6 6e-6 1.2e-5 2.4e-5 4.8e-5
ppbv/grid cell

Figure 9

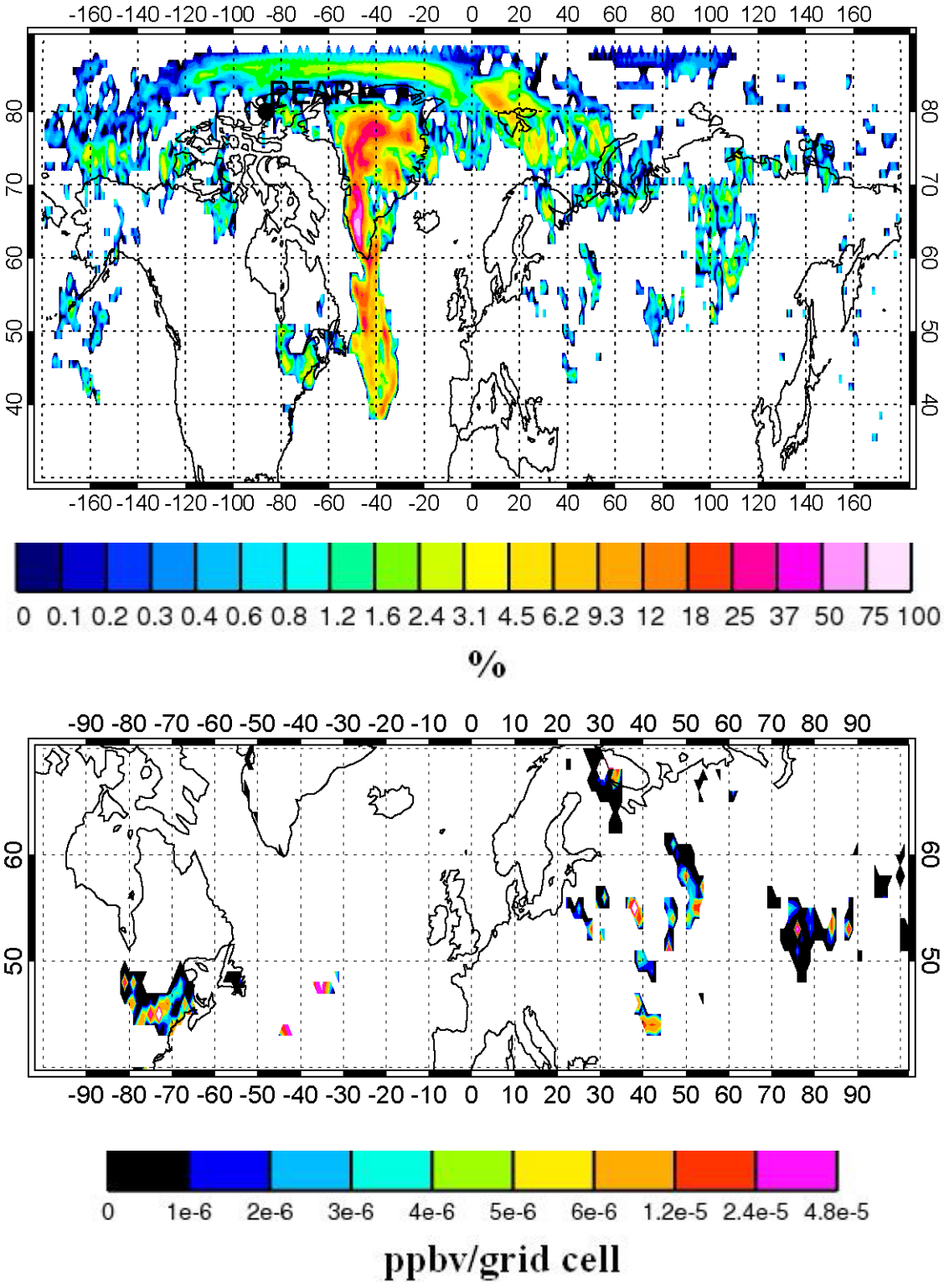
-160 -140 -120 -100 -80 -60 -40 -20 0 20 40 60 80 100 120 140 160
80
70
60
50
40
PEARL
0 0.1 0.2 0.3 0.4 0.6 0.8 1.2 1.6 2.4 3.1 4.5 6.2 9.3 12 18 25 37 50 75 100
%
-90 -80 -70 -60 -50 -40 -30 -20 -10 0 10 20 30 40 50 60 70 80 90
60
50
0 1e-6 2e-6 3e-6 4e-6 5e-6 6e-6 1.2e-5 2.4e-5 4.8e-5
ppbv/grid cell

Figure 10

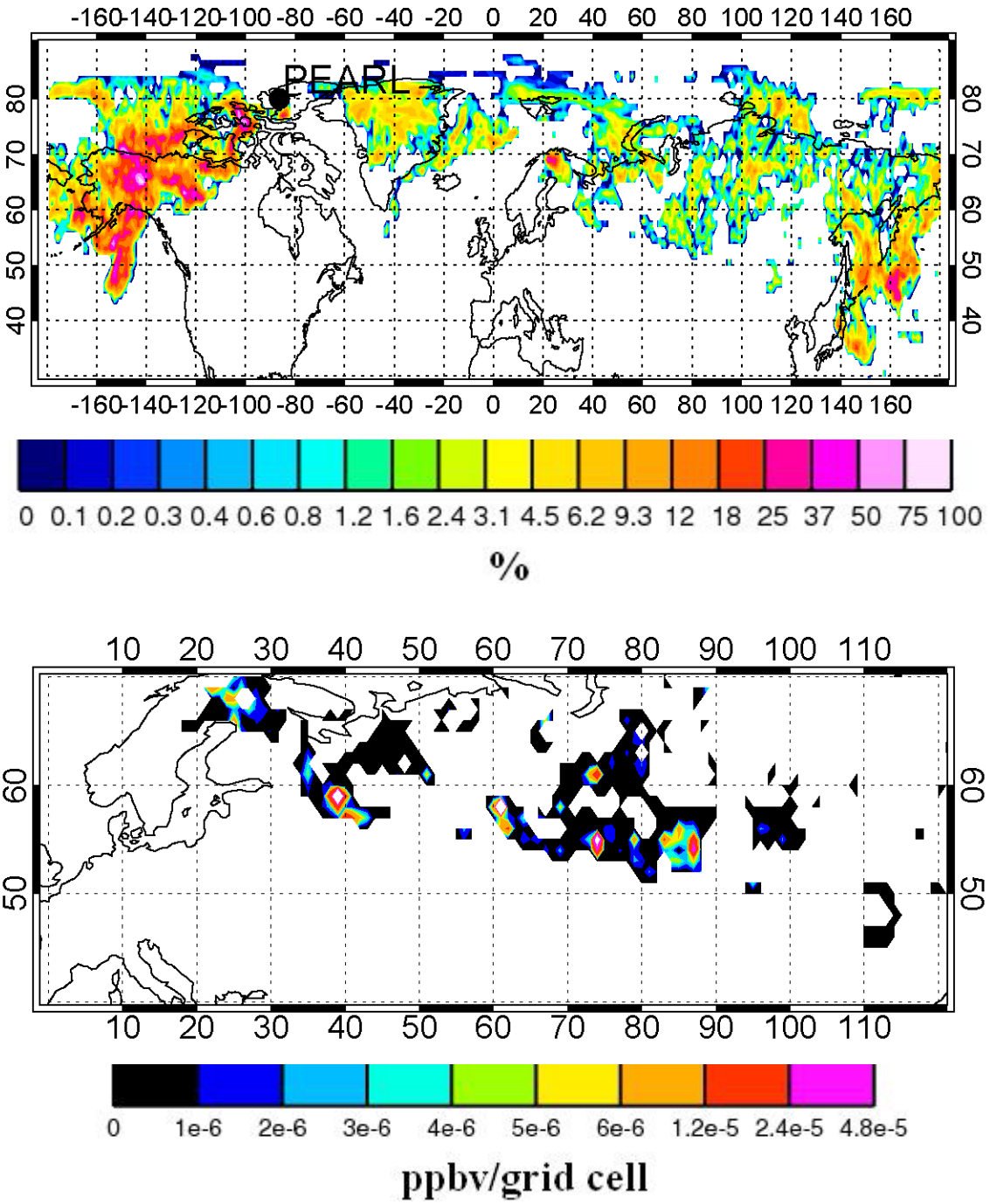
-160 -140 -120 -100 -80 -60 -40 -20 0 20 40 60 80 100 120 140 160
PEARL
80 70 60 50 40
0 0.1 0.2 0.3 0.4 0.6 0.8 1.2 1.6 2.4 3.1 4.5 6.2 9.3 12 18 25 37 50 75 100
%
10 20 30 40 50 60 70 80 90 100 110
60 50
0 1e-6 2e-6 3e-6 4e-6 5e-6 6e-6 1.2e-5 2.4e-5 4.8e-5
ppbv/grid cell

Figure 11

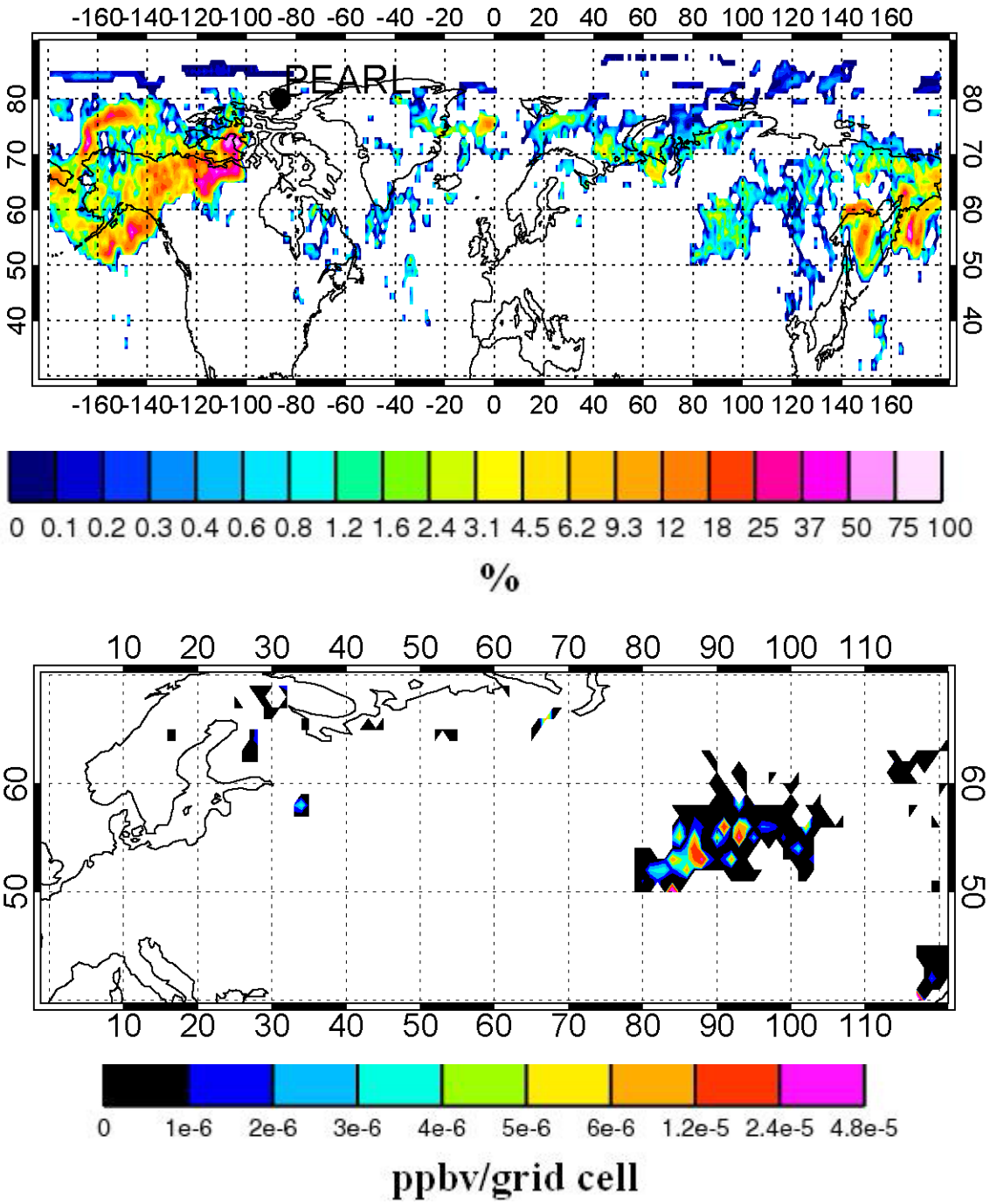
-160 -140 -120 -100 -80 -60 -40 -20 0 20 40 60 80 100 120 140 160
PEARL
80 70 60 50 40
0 0.1 0.2 0.3 0.4 0.6 0.8 1.2 1.6 2.4 3.1 4.5 6.2 9.3 12 18 25 37 50 75 100
%
10 20 30 40 50 60 70 80 90 100 110
60 50
0 1e-6 2e-6 3e-6 4e-6 5e-6 6e-6 1.2e-5 2.4e-5 4.8e-5
ppbv/grid cell

Figure 12